CHAPTER 5
EXTRACTIVE DESULFURIZATION OF SELECTED IONIC LIQUIDS

5.0 Overview

This chapter provides the results on extractive desulfurization starting from evaluation using model oil up to actual diesel. The validation of AI and DBE against experimental result (K_d value) using model oil are firstly discussed. Mapping and correlation towards K_d value using model oil along with ternary diagram of BT, [bmim][TCM] and hydrocarbons plus regeneration study are also included.

5.1 Validation Study of AI and DBE assisted COSMO-RS

25 ILs were synthesized accordingly (refer to Table 5.1), and their desulfurization performance were determined in terms of K_d value. As mentioned earlier, K_d value refer to the mobility of BT or sulfur compounds from raffinate phase transferred to extractant phase during extraction process.

From the pattern of AI values, it is apparent that the order is as follows: imidazole ≈ pyrazole > benzimidazole > pyridine > pyrrolidine. Meanwhile, the results from extractive desulfurization depicted the order differently, as shown in Figure 5.1. The inconsistent order between AI and K_d values was found to be due to the physical phase of ILs. Benzimidazole-based ILs are in the solid form at room temperature, resulting in poor desulfurization performance (K_d value = 0.124). As part of our study on screening of ILs for desulfurization, physical phase is an important aspect that should be considered first before evaluating respective AI for cation selection.

Table 5.1: Selected combination of cation and anion for ionic liquids with their respective calculated AI and DBE values

Cation		Anion		K_d value at
Acronym	**AI value**	**Acronym**	**DBE value**	**25.5°C**
mmim	2	MSO_4	0.5	0.409
mmpyz	2	MSO_4	0.5	0.366
mmBzim	1	MSO_4	0.5	0.124
mmpy	0.875	MSO_4	0.5	0.334
mmpyrr	0	MSO_4	0.5	0.306
bmim	2	DHP	0.5	0.191
bmim	2	DMP	0.5	1.439
bmim	2	DBP	0.5	1.703
bmim	2	HSO_4	0.5	0.205
bmim	2	MSO_4	0.5	1.222
bmim	2	BSO_4	0.5	1.500
bmim	2	OSO_4	0.5	2.030
bmim	2	OTf	0.5	0.942
bmim	2	NTf_2	0.5	1.273
bmim	2	Ac	1.5	1.564
bmim	2	TFA	1.5	1.500
bmim	2	NO_3	1.5	1.500
bmim	2	CNS	2.5	1.857
bmim	2	Imd	3.5	2.125
bmim	2	Pyd	3.5	2.030
bmim	2	TOS	4.5	0.471
bmim	2	DCA	4.5	2.448
bmim	2	BZT	5.5	2.846
bmim	2	SCL	5.5	2.571
bmim	2	TCM	6.5	3.762

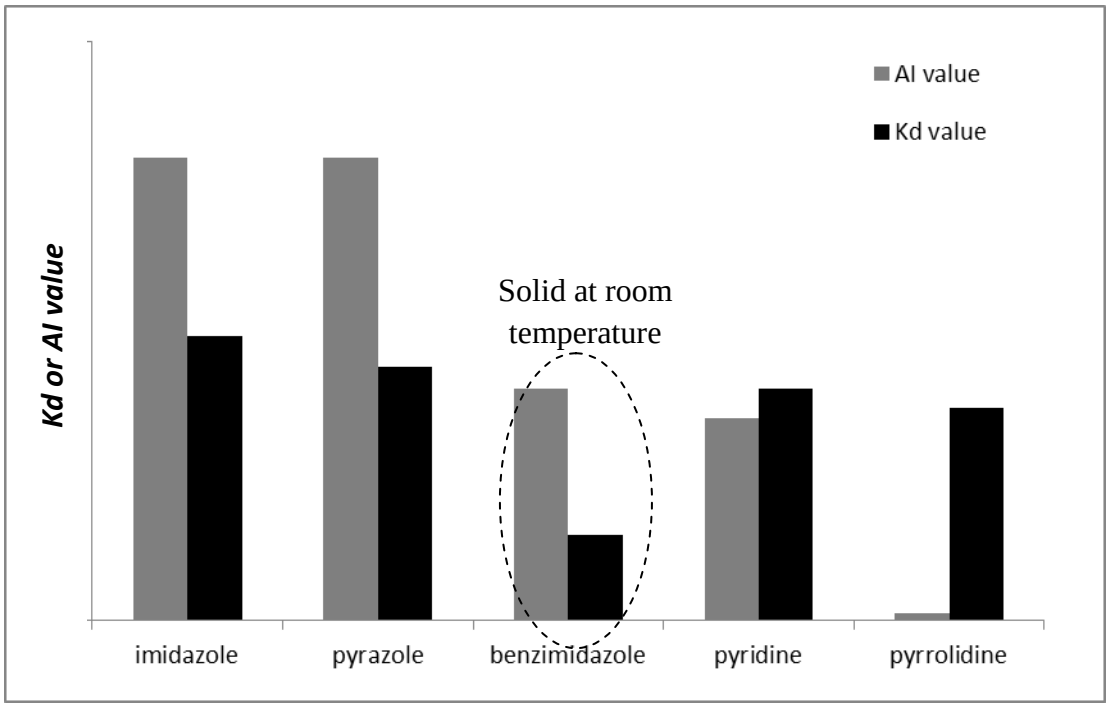

Figure 5.1: Comparison of AI value and desulfurization partition coefficient (K_d value) of cations

In the second part of the ILs prediction for desulfurization, it should be noted that all of the ILs used are composed of relatively similar cations. Table 5.1 reports the experimental K_d values of 20 ILs at room temperature along with their respective DBE values, which are also illustrated in Figure 5.1. The DBE value agrees reasonably well with the experimental findings if 1-butyl-3-methylimidazolium tosylate (TOS) is excluded. The desulfurization ability of this IL on model oil is reduced due to its solid phase nature. Within the same root of anion (as referred to dihydrogenphosphate (DHP), dimethylphosphate (DMP) and dibutylphosphate (DBP), hydrogensulfate (HSO_4), methylsulfate (MSO_4), butylsulfate (BSO_4) and octylsulfate (OSO_4)), anions that have longer alkyl chains gave higher performances. Weakening of anions due to alkyl chain length can be correlated to the strength of cation-anion interactions whereby the shorter the alkyl chain, the stronger the interaction between cation-anion. Mochizuki and Sugawara (2008) observed a similar trend in their work where the extraction of sulfur compound increases linearly with the increase in alkyl chain length of imidazolium-based sulfate ILs. Among the ILs, tricyanomethane (TCM) stands out with a K_d value of 3.762. This is closely followed

by benzoate (BZT) and salicylate (SCL) anion with K_d values of 2.846 and 2.571, respectively.

Further analysis found that there was strong proportional relationship between classified DBE with average K_d value, as shown in Figure 5.3. The analysis was done by excluding [bmim][TOS] due to solid state of this ILs, resulted poor desulfurization performance. This proves that by determining AI and DBE values, which are not covered by COSMO-RS under non-polar region, potential ILs for desulfurization process can be identified.

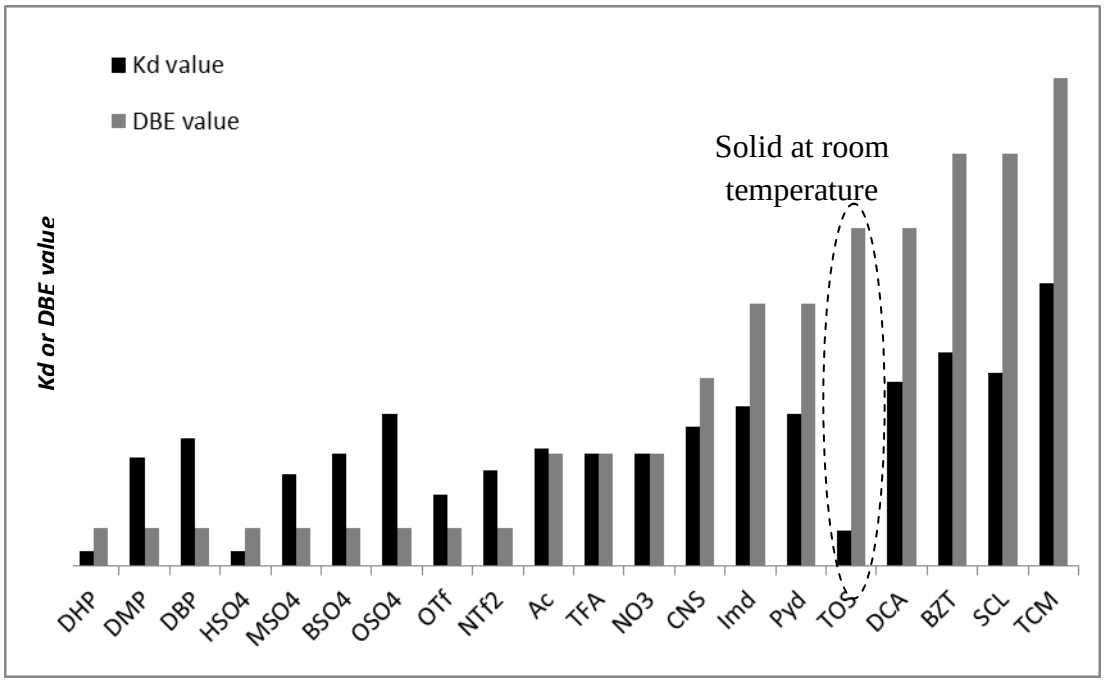

Figure 5.2: Comparison of DBE value and desulfurization partition coefficient (K_d value) of anions

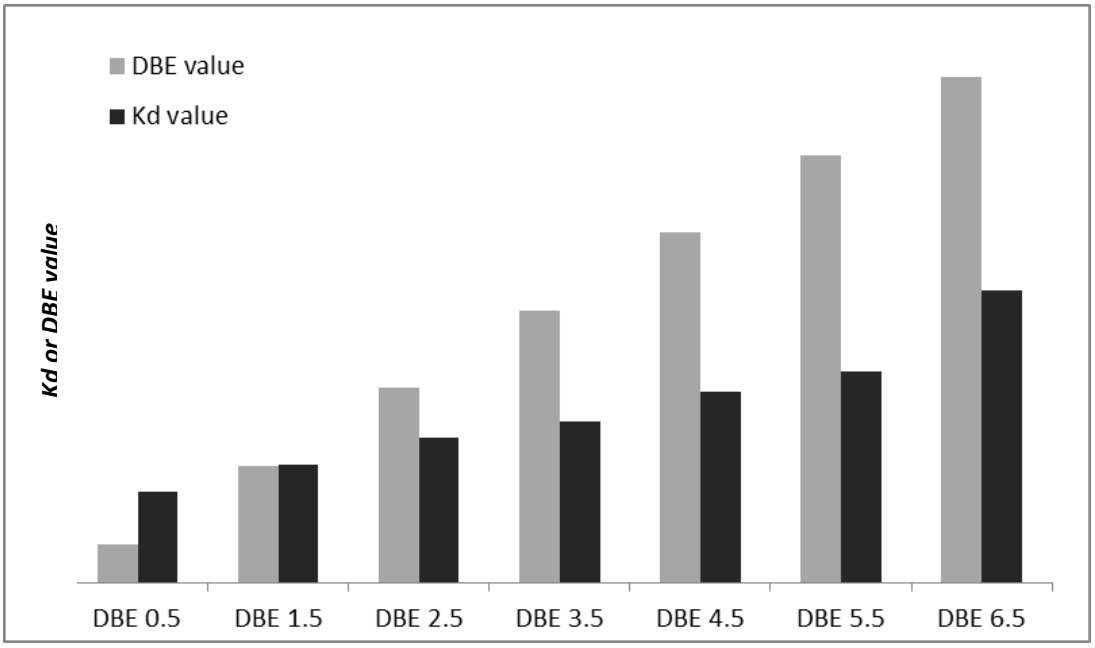

Figure 5.3: Classified DBE value and average K_d value of anions

5.2 Mapping and Correlation Study

A statistical analysis using MATLAB software package was applied to 23 ILs where three basic physical properties namely molecular weight, density and refractive index, which are independent of each other, have been considered, to establish their relationships with desulfurization performance. Two ILs namely [mmBzim][MSO_4] and [bmim][TOS] were not attempted for statistical analysis due to their existence in solid state form.

The aim of this mapping and correlation study is to show that the plot of original density data (ρ) against the molecular weight (M_W) can provide a quick indication of the relationship between the variables if the classification of the data is done correctly. In addition, the plot would easily show any outliers or other aberrations among the data. In this study, the original data were plotted as shown in Figure 5.4, and the variables used in constructing data plot were tabulated as shown in Table 4.8. For easy pattern justification of the data plot, the data are categorized into two groups depending on their partition coefficient, K_d which defines the extent of mobility of BT (sulfur compound) into ILs phase; the values were taken from previous screening

section. Desulfurization performance can be identified from the K_d value; i) $K_d > 1$ indicates that the BT removal from model oil is more than 50% and ii) $K_d < 1$ indicates that the removal is less than 50%. This value has become an important benchmark in this study as the basic selection criteria for categorizing ILs.

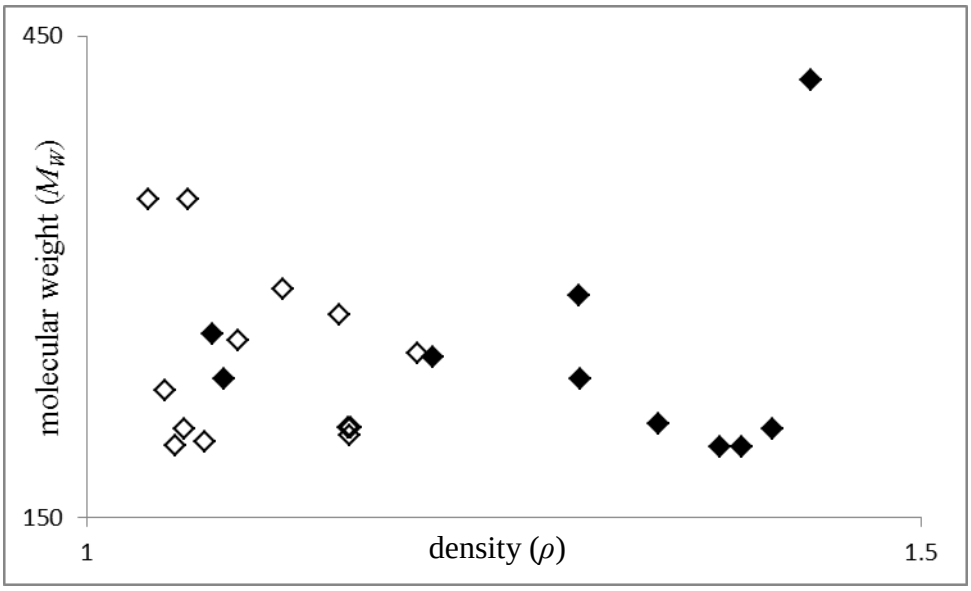

Figure 5.4: Graphical presentation for original data of 23 ILs of density (ρ) against molecular weight (M_W), where fill-dotted $K_d > 1.5$ while others $K_d < 1.5$

Table 5.2: List of ILs with their respective physical properties and desulfurization performance

ILs	Synthesized			
	ρ *(g/cm^3)*	n_D	M_W *(g/mol)*	K_d
[mmim][MSO_4]	1.2980	1.4638	208.24	0.409
[mmpyz][MSO_4]	1.3927	1.4688	208.24	0.366
[mmpy][MSO_4]	1.4114	1.5238	236.33	0.334
[mmpyrr][MSO_4]	1.3078	1.4487	211.28	0.306
[bmim][DHP]	1.0822	1.4534	236.21	0.191
[bmim][DMP]	1.0751	1.4790	264.26	1.439
[bmim][DBP]	1.0372	1.5046	348.42	1.703
[bmim][BSO_4]	1.1140	1.4757	292.40	1.500
[bmim][Imd]	1.1580	1.5151	206.29	2.125
[bmim][Pyd]	1.1571	1.5275	206.29	2.030
[bmim][BZT]	1.0905	1.5236	260.33	2.846
[bmim][SCL]	1.1515	1.5367	276.33	2.571
	Purchased			
[bmim][HSO_4]	1.2958	1.4706	236.29	0.205
[bmim][MSO_4]	1.2082	1.4712	250.32	1.222
[bmim][OSO_4]	1.0606	1.4907	348.51	2.030
[bmim][OTf]	1.2815	1.4380	288.29	0.942
[bmim][NTf_2]	1.4343	1.4263	422.38	1.273
[bmim][Ac]	1.0527	1.4742	195.24	1.564
[bmim][TFA]	1.1980	1.4455	252.23	1.500
[bmim][NO_3]	1.1539	1.5059	201.22	1.500
[bmim][CNS]	1.0704	1.5081	197.31	1.857
[bmim][DCA]	1.0581	1.5096	205.26	2.448
[bmim][TCM]	1.0467	1.5335	229.28	3.762

Figure 5.4 presents the plotted data which shows scatterings of all types of ILs within the range of study as the desulfurization process was carried out. This leads to the observation that all 23 types of ILs showed no discernible pattern for separation in terms of desulfurization performance. On the other hand, when the same data were categorized based on the chemical structure of the ILs anion and re-plotted, clear separation regions can be observed, as shown in Figure 5.5. The five classifications identified in this figure are cyano-based ILs, phosphate-based ILs, fluoro-based ILs, sulfate-based ILs (correlation line with R^2 = 0.9175) and others, including [bmim][NO_3], [bmim][Ac], [bmim][Imd], [bmim][Pyd], [bmim][BZT] and [bmim][SCL] which cannot be grouped. Meanwhile, the sulfate-based ILs formed a straight line on the ρ against M_W plot using the data of eight ILs. For further analysis,

the classifications of individual ILs will be discussed in details after the data have been normalized.

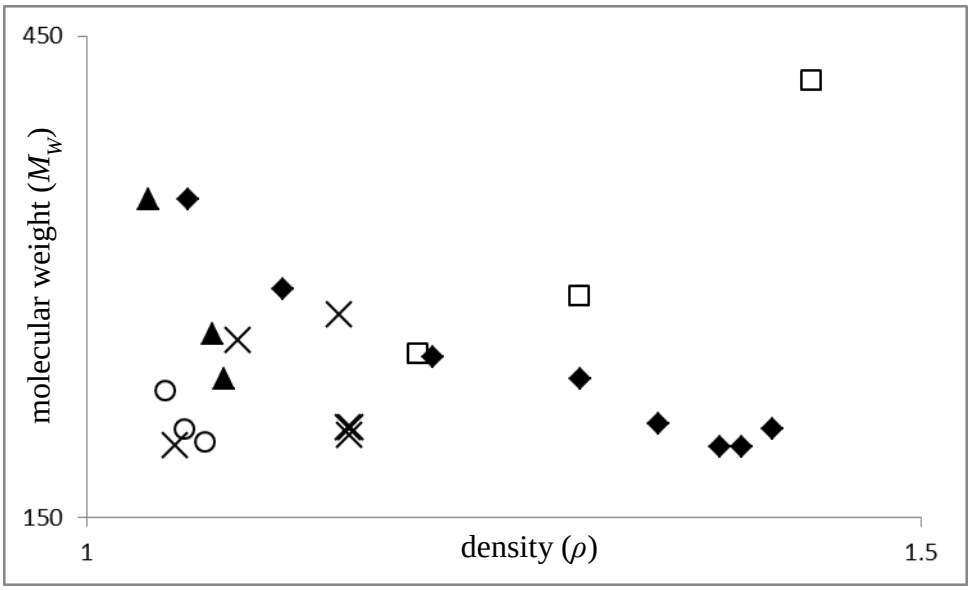

Figure 5.5: Graphical presentation of original data of the 23 ILs of density (ρ) against molecular weight (M_W) with identified group; (cyano-based ILs, circle plot; phosphate-based ILs, filled-triangle plot; fluoro-based ILs, rectangular plot; sulphate-based ILs, filled-rectangular plot)

The cyano-based ILs consisted of [bmim][CNS], [bmim][DCA] and [bmim][TCM] where their chemical structures presented in Figure 5.6. Referring to the experimental results of the extractive desulfurization performance (refer to Table 5.2), it is observed that K_d value increases with increasing number of cyano group (−C≡N) uptick on the anion structures and the order is as follows: CNS < DCA < TCM. Figure 5.7 shows the normalized data of ρ against M_W plot. By comparing the linear correlation line and the desulfurization performance of cyano-based ILs, a similar trend is apparent where TCM can be found at the top spot of the correlation followed by DCA and CNS, as shown in Figure 5.7. The great thing about this similarity is that, it could possibly become the predictive mapping for a new generation of IL that consists of cyano group, to be used purposely for diesel desulfurization, just by plotting ρ against M_W.

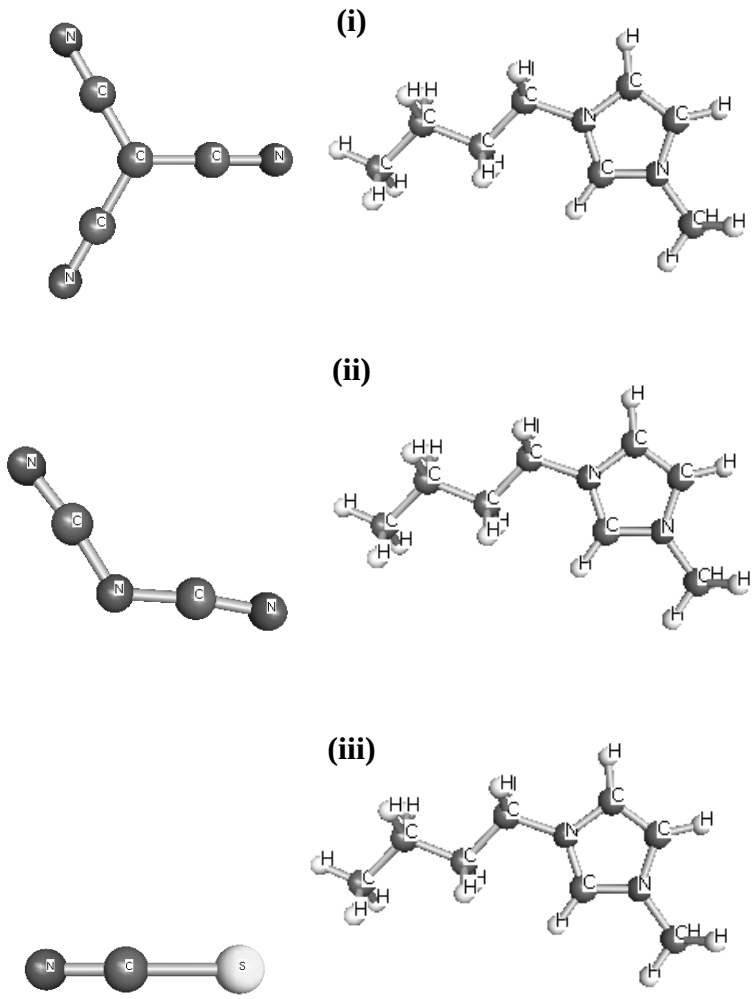

Figure 5.6: Chemical structures of cyano-based ILs: (i) [bmim][TCM], (ii) [bmim][DCA], and (iii) [bmim][SCN]

The second classified group is phosphate-based ILs which consists of three compounds, namely [bmim][DHP], [bmim][DMP] and [bmim][DBP]. The experimental results from the desulfurization performance revealed that K_d value decreases as the number of alkyl chain is lost on both the cation and anion parts, which follows the order of DBP > DMP > DHP. It can be explained that by losing the alkyl chain, the Coulombic attraction between the cation and the anion of the ILs became stronger, thus hindering the interaction between the sulfur compound and the ILs. Figure 5.8 depicts the normalized data of ρ against M_W plot. It seems obvious that the linear correlation of phosphate-based ILs followed the same order of

desulfurization performance trend. This mapping could become one of the simplified methods in the search for a new phosphate-based IL for diesel desulfurization.

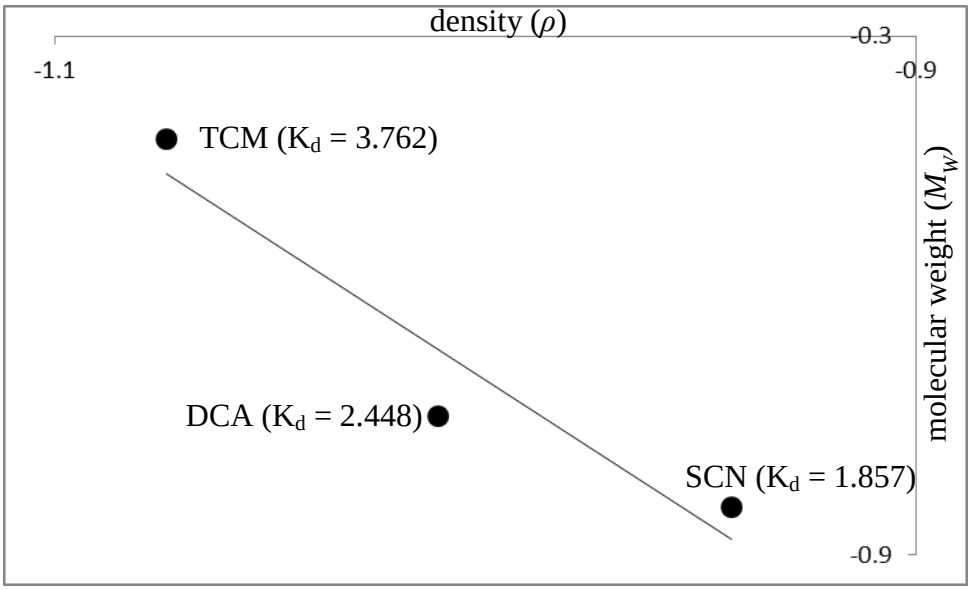

Figure 5.7: Standardized data of density (ρ) plotted against molecular weight (M_W) of ILs with cyano-based ILs

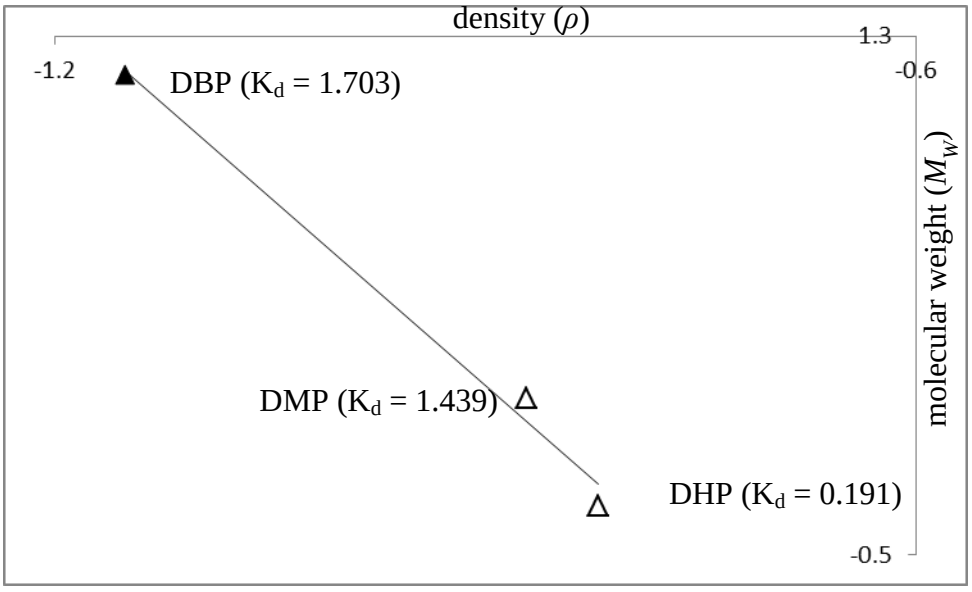

Figure 5.8: Standardized data of density (ρ) plotted against molecular weight (M_W) of ILs with phosphate-based ILs

The fluoro-based ILs also consists of three compounds namely [bmim][OTf], [bmim][NTf_2] and [bmim][TFA], and the order of their desulfurization performance is TFA > NTf_2 > OTf. It seems there is no clear explanation regarding the behaviour of this group either on physical properties or chemical structure however, they correlated linearly between ρ and M_W as shown in Figure 5.9.

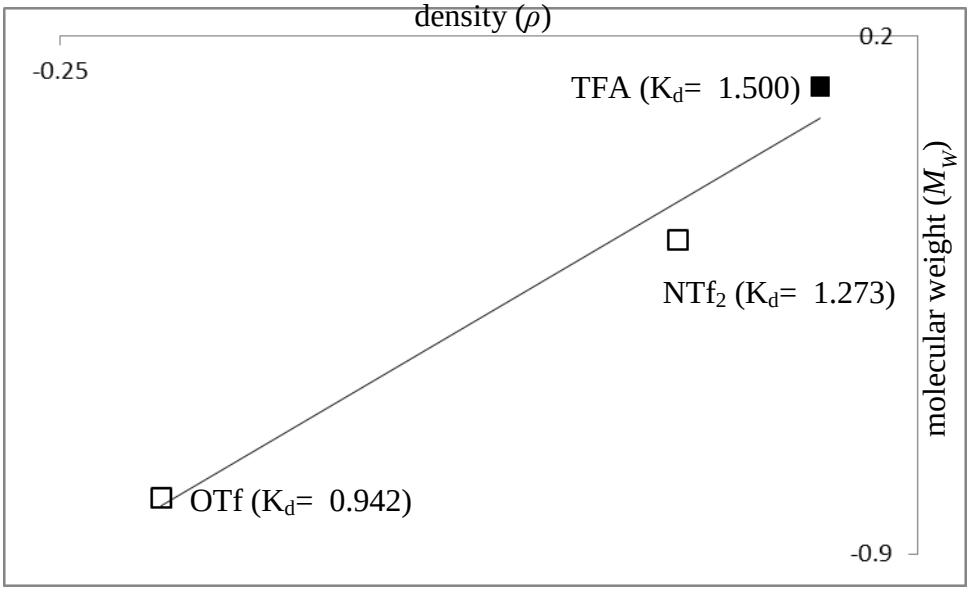

Figure 5.9: Standardized data of density (ρ) plotted against molecular weight (M_W) of ILs with fluoro-based ILs

It is observed that the ILs in the classified groups interacted in a parallel behaviour (having characteristics in common), as apparent by the patterns seen on the groups' plotted data. Upon inspection, the largest classified group which was the sulfate-based ILs had also shown a linear correlation, as seen in Figure 5.10. The plot depicts on the upper side of the linear correlation, as represented by filled-dots, are the ILs with K_d values greater than 1.5 while on the lower side, depicted by unfilled-dots, are the ILs with K_d values of less than 1.5. A parallel behaviour can be observed in Figures 5.7, 5.8, 5.9 and 5.10 where the best ILs in each group is plotted at the top of their correlations. By introducing these four mappings, an easier method may has been demonstrated, for identifying potential ILs for diesel desulfurization, which could become significant especially in the petroleum industry.

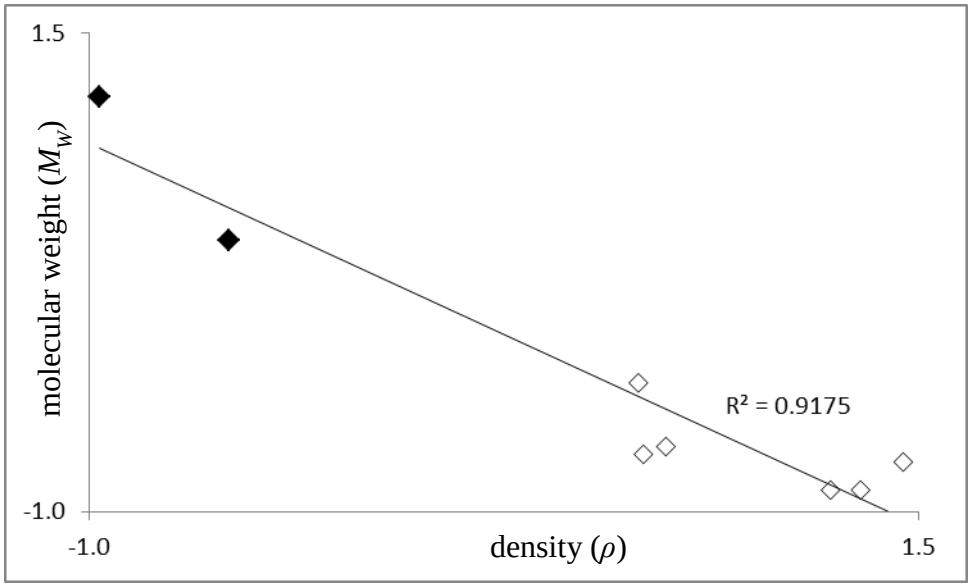

Figure 5.10: Standardized data of density (ρ) plotted against molecular weight (M_W) of sulfate-based ILs, R^2 = 0.9175, (filled-dots represent K_d > 1.5 while others represent K_d < 1.5)

5.3 Extractive Desulfurization Study on Model Oil

In this study, experiments were conducted for the removal of sulfur compound (present as BT) with concentration of 2000 ppm in the model oil (present as *n*-dodecane) using 1-butyl-3-methylimidazolium tricyanomethane ([bmim][TCM]) as the extractant. Suggested by AI and DBE assisted COSMO-RS, and based on validation study, [bmim][TCM] showed the most potential to further investigate for extractive desulfurization study on model oil. The effects of stirring speed, extraction time and water content on the extraction efficiency were investigated. At the end of this part, the loading factor of the [bmim][TCM] is also discussed.

5.3.1 Effect of Stirring Speed

The effect of stirring speed on sulfur extraction efficiency (K_d value) was firstly investigated. As shown in Figure 5.11, there is a drastic extraction efficiency increment with an increase of stirring speed from stagnant to 100 rpm. A very low extraction occurred during the stagnant period where only interfacial extraction of both oil and ILs took place. Then the K_d value continued to linearly increase with the

increase of stirring speed from 100 rpm to 500 rpm. As mentioned before in Chapter 3, the maximum allowable speed of the extractor vial is 500 rpm, therefore the experiment was limited to 500 rpm as the optimum stirring speed in order to achieve higher sulfur extraction efficiency.

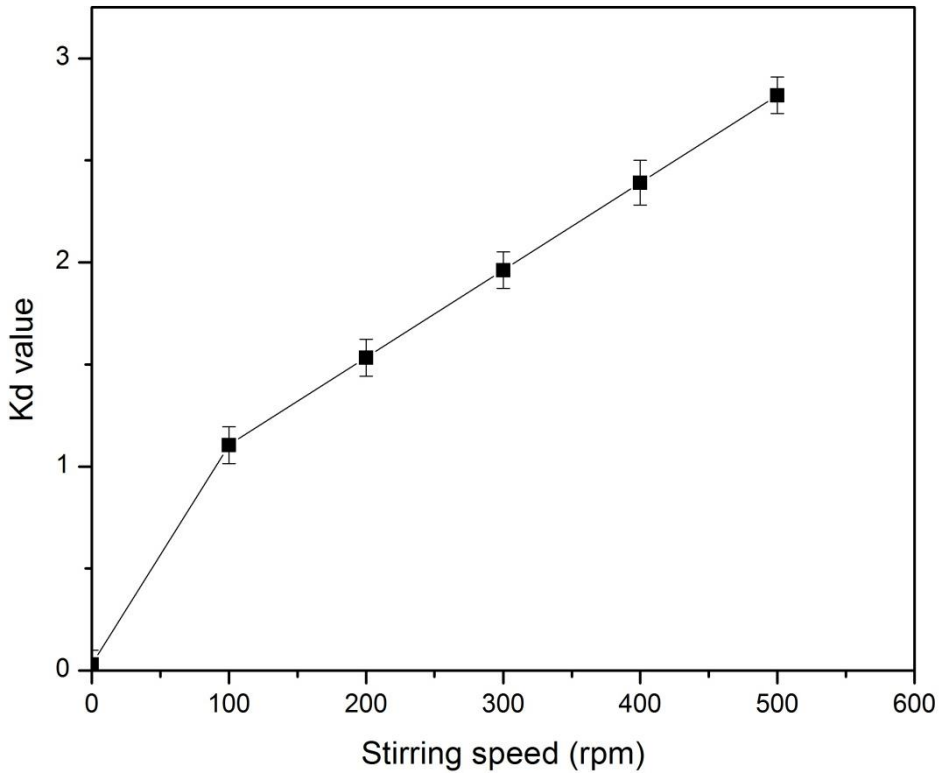

Figure 5.11: The effect of stirring speed on sulfur extraction efficiency (K_d value) by [bmim][TCM]. *(Conditions: Extraction time – 10 min, mass ratio ILs/model oil – 1/1, room temperature, initial BT concentration in model oil – 2000 ppm)*

5.3.2 Effect of Extraction Time

In an effort to understand the effect of extraction time, experiments were repeated at the optimum stirring speed condition and the results are displayed in Figure 5.12. As can be seen from Figure 5.12, the sulfur extraction efficiency increased with an increase in extraction time for the first 30 minutes. Extending the extraction time longer than 30 minutes did not result in extracting more BT from the model oil phase, indicating that the extraction process has reached equilibrium state. Similar results were obtained by other researchers, where the required extraction time ranged from 25 min to 30 min (*Liu[b] et al. 2008; Taib and Murugesan, 2011*). It was also observed

that there is no marginal increase in extraction efficiency by increasing the extraction time of unstirred samples.

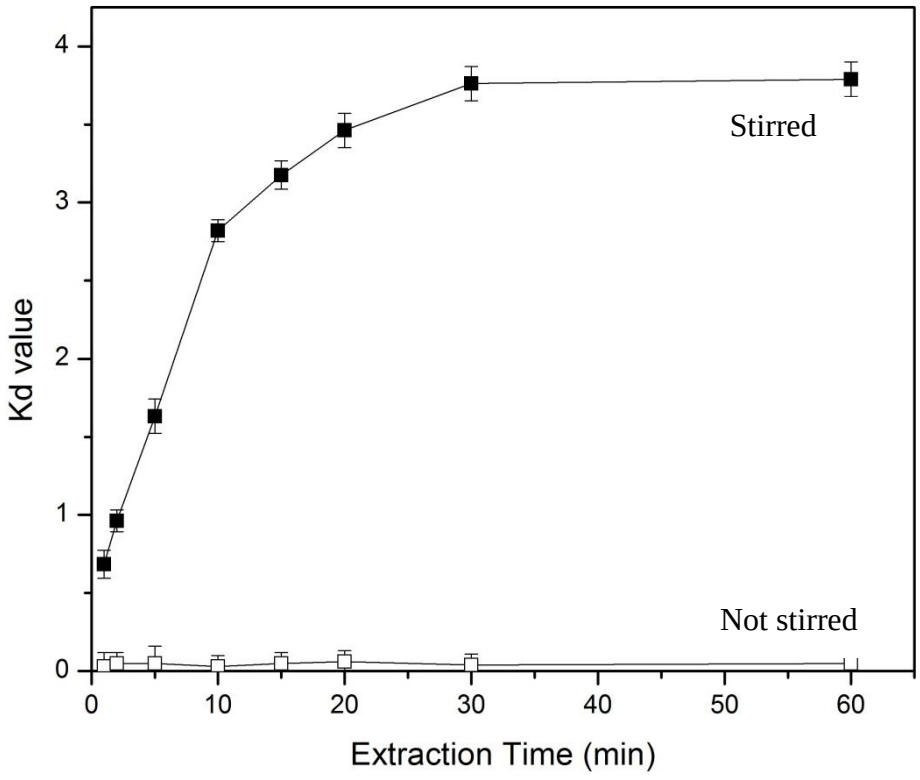

Figure 5.12: The effect of extraction time on sulfur extraction efficiency (K_d value) by [bmim][TCM] *(Conditions: Stirring speed – 500 rpm, mass ratio ILs/model oil – 1/1, room temperature, initial BT concentration in model oil – 2000 ppm)*

5.3.3 Effect of Water Content

As shown in Figure 5.13, the sulfur extraction efficiency decreased dramatically as the water content in [bmim][TCM] increased, for instance 2.5% of water content in [bmim][TCM] can drop the K_d value by about 1.5 from 3.672 at 0.000233% (233 ppm) water content. This implies that the efficiency of BT extraction using [bmim][TCM] from the model oil decreases drastically with the presence of more water in [bmim][TCM]. On the other hand, this also suggests that the sulfur compounds dissolved in the spent ILs can be regenerated by water dilution process, which will be later discussed in the regeneration segment.

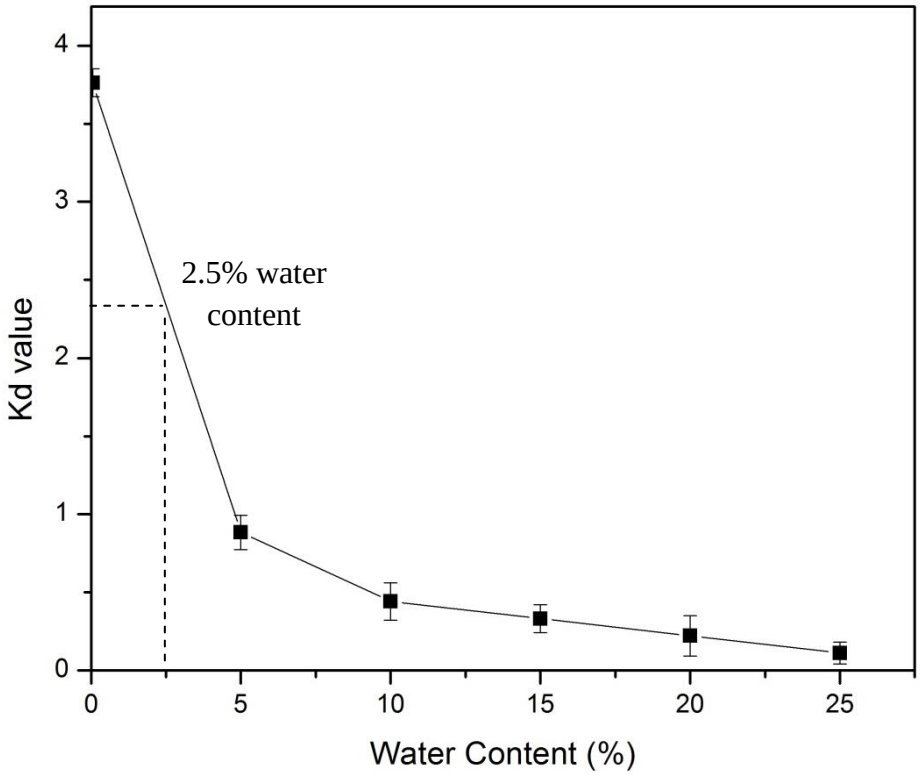

Figure 5.13: The effect of water content on sulfur extraction efficiency (K_d value) by [bmim][TCM]. *(Conditions: Stirring speed – 500 rpm, extraction time – 30 min, mass ratio ILs/model oil – 1/1, room temperature, initial BT concentration in model oil – 2000 ppm)*

5.3.4 Effect of Concentration of [bmim][TCM] on Extraction

The choice of a suitable composition for the ILs (extractant) was carried out experimentally, and [bmim][TCM] was chosen. The effect of [bmim][TCM] concentration in water, as the extracting solvent, on sulfur extraction efficiency is shown in Figure 5.14. A drastic reduction in K_d value can be seen as the [bmim][TCM] concentration dropped from 4.36 mM to 4.14 mM; but, from 3.93 mM down to 3.27 mM of [bmim][TCM] concentration, the K_d value was linearly reduced. This suggests that at the initial stage of extraction process, which shows major influence toward extraction efficiency, the presence of water in [bmim][TCM] should be avoided. In the presence of both water and BT, the interaction of ILs is much more favourable for water instead of BT via hydrogen bonding, by means a stronger interaction than π-π bonding.

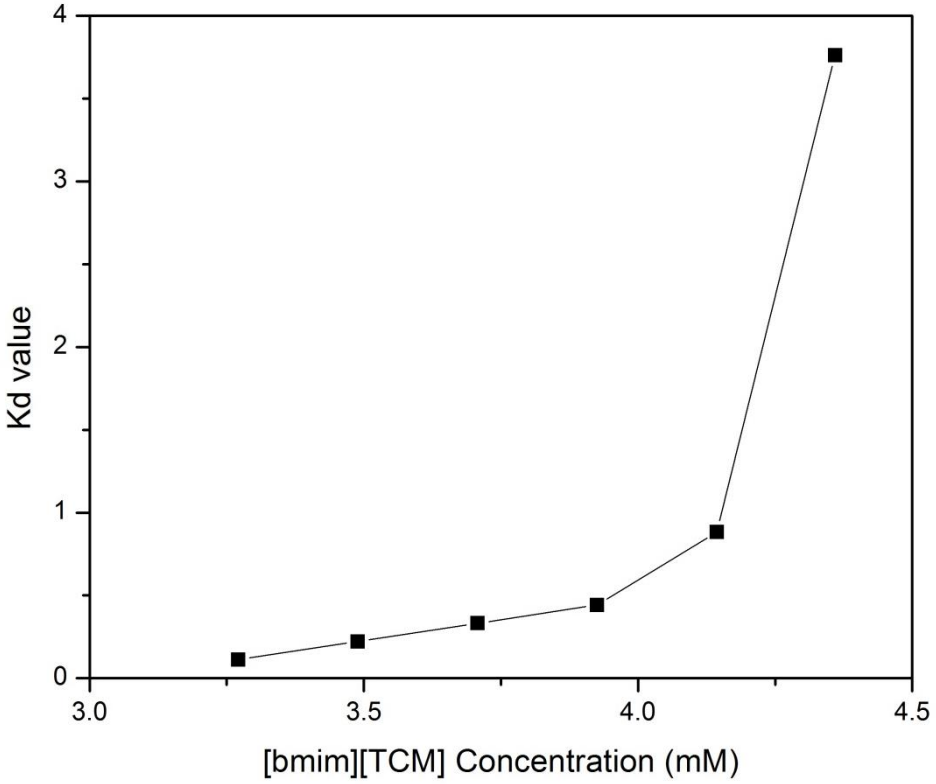

Figure 5.14: Relationship between K_d value and [bmim][TCM] concentration

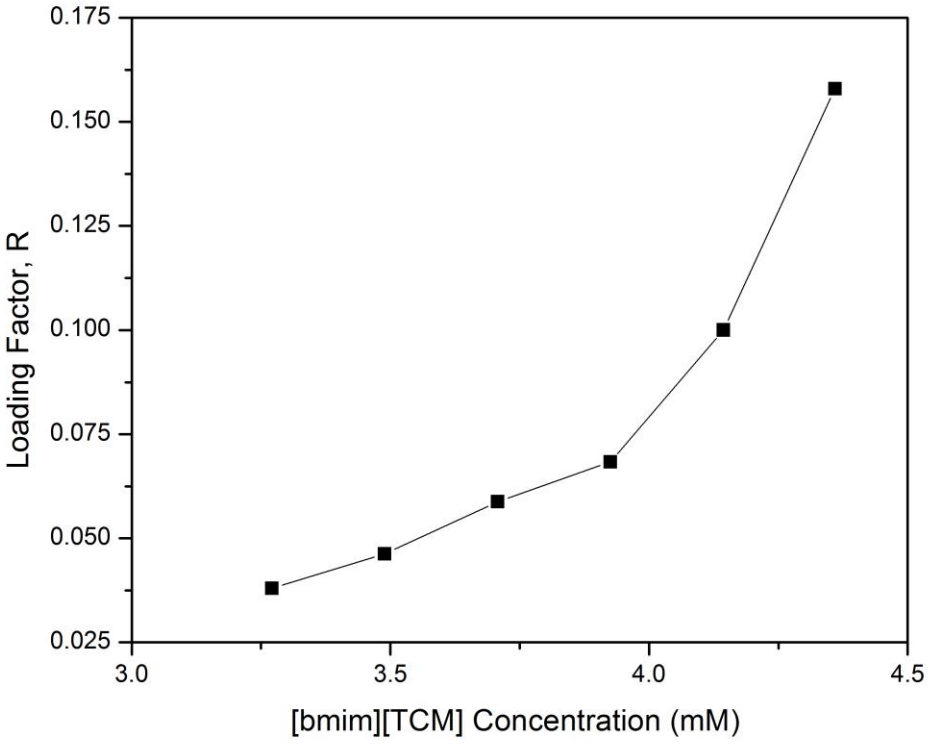

Figure 5.15: Relationship between loading factor and initial concentration of [bmim][TCM] *(Conditions: Stirring speed – 500 rpm, extraction time – 30 min, mass ratio ILs/model oil – 1/1, room temperature, initial BT concentration in model oil – 2000 ppm)*

In the case of loading factor, when R > 1 it is called overloading. It means that more than two moles of solutes (represented by BT) react with one mole of extractant (represented by ILs). On the other hand, in the case of R < 1, it means that several mole of extractant interact with one mole of solute (*Yunhai et al. 2006*). As seen in Figure 5.15, at any point the R values for BT extraction is lower than 1. This indicates that more than one mole of [bmim][TCM] may interacted with one mole of BT during the desulfurization process.

5.4 Optimization using RSM

5.4.1 Regression Analysis

The experimental results obtained to fit the quadratic model (i.e. Eq. 2.1) for the various points as per the experimental design are summarized in Table 5.3. Percentage of BT removed (% removal) was chosen instead of K_d value for better understanding of the optimization study.

Table 5.3: Experimental design result for BT removal

Factor (coded value)			% removal (response)	
A	**B**	**C**	**Observed**	**Predicted**
+1	-1	+1	85	86.16
+1	+1	+1	81	81.74
-1	-1	-1	66	65.56
0	0	0	79	80.54
-1	-1	+1	69	68.16
+1	+1	-1	80	81.16
0	-1	0	81	83.76
0	0	-1	77	76.55
-1	0	0	64	68.35
0	0	0	80	80.54
0	0	0	81	80.54
0	0	0	78	80.54
+1	0	0	93	86.35
-1	+1	-1	65	63.16
0	0	0	79	80.54
+1	-1	-1	82	83.56
-1	+1	+1	67	65.76
0	0	0	86	80.54
0	+1	0	78	79.34
0	0	+1	81	79.15

Table 5.4 tabulated the quadratic model significance and the corresponding significant terms of the model response. The relationship between the response and the factor variables is found to be non-linear using ANOVA. The first order (A) and second-order (A^2) terms for the mass ratio (model oil/ILs) appear to be significant in influencing the response variable i.e. percentage of BT removed. The initial concentration (B) and temperature (C) were also included in the analysis for the purpose of evaluating their significance in influencing the response variable. However, the results obtained show that the effect was not significant within this range of study. The finding from the regression study also reveals that there was no

apparent interaction between the three variables. This is confirmed by the parallelism trend as shown in Figure 5.16 (a), 5.16 (b) and 5.16 (c) on the change of the average response displayed in one factor plot, graphically indicating the absence of interaction effect between the main factors studied. Consequently, the main contribution to the response of the generated quadratic model is only from mass ratio.

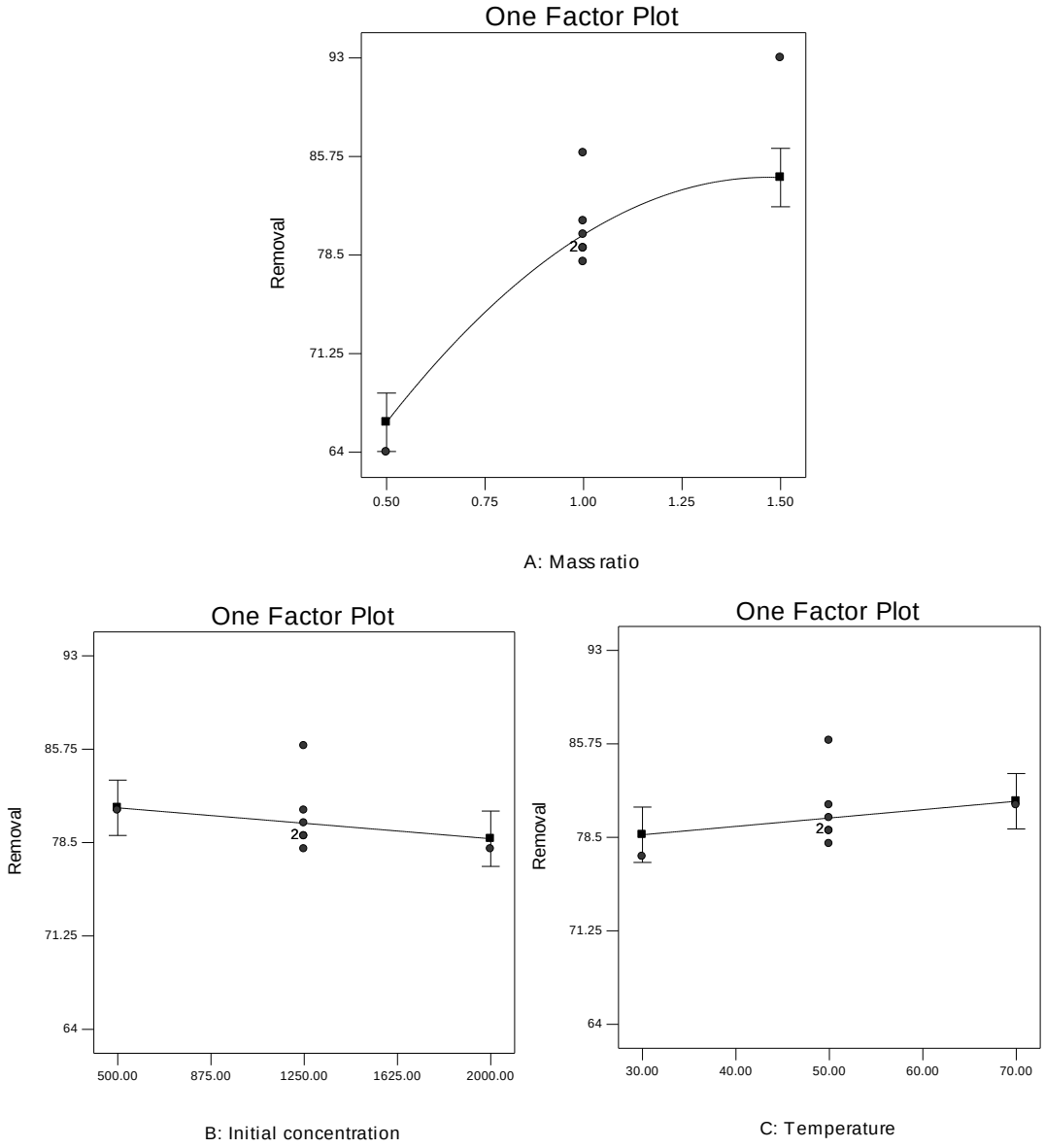

Figure 5.16: One factor plot for (a) mass ratio, (b) initial concentration and (c) temperature against average response

Table 5.4: ANOVA of the reduced quadratic regression model and respective model terms

Source	Sum of squares	d.f.	Mean squares	F-value	Prob. > F
Quadratic	956.50	4	239.13	23.55	< 0.0001[a]
A	810.00	1	810.00	79.78	< 0.0001[a]
B	14.40	1	14.40	1.42	0.2522
C	16.90	1	16.90	1.66	0.2165
A^2	115.20	1	115.20	11.35	0.0042[a]
Lack of fit	110.80	10	11.08	1.33	0.3949[b]
Pure error	41.50	5	8.30		

[a] Significant under 95% level of confidence
[b] Not significant relative to pure error due to noise

Based on ANOVA analysis tabulated in Table 5.4, a reduced quadratic regression model expressed by Eq. 5.1 was then developed. A, B, C and Y represents the mass ratio, initial concentration, temperature and removal of BT in percentage, respectively.

$$\mathbf{Y = 80.00 + 9.00A - 1.20B + 1.30C - 4.80A^2} \quad (5.1)$$

Statistical parameters obtained from ANOVA for the reduced models of the BT removal process are given in Table 5.5. The coefficient of variance (CV) for the reduced model representing BT removal was found to be 4.11%. The CV is taken as the ratio of the estimated standard error to the mean value of the observed response which is a measure of reproducibility of the model. As a general rule, the model can be considered as reasonably reproducible if the CV value is not greater than 10%. While the adequate precision value is a measure of "signal-to-noise ratio" encountered on the measurement of the response. A ratio greater than 4 is considered to be adequate for model discrimination [Montgomery, 2003]. In this work, the adequate precision for the response is 14.44 which are well above 4. The value of R^2 = 0.8626 was found to be reasonably high, confirming the accuracy of the model. The accuracy of the model is further illustrated by plotting the predicted versus experimental value as shown in Figure 5.17. It clearly shows a good agreement between the two data.

Table 5.5: Statistical parameters obtained from ANOVA for the reduced quadratic regression model

Variable	% removal
R^2	0.8626
R^2 adjusted	0.8260
Standard deviation (S.D.)	3.19
Coefficient of variance	4.11
Adequate precision	14.436

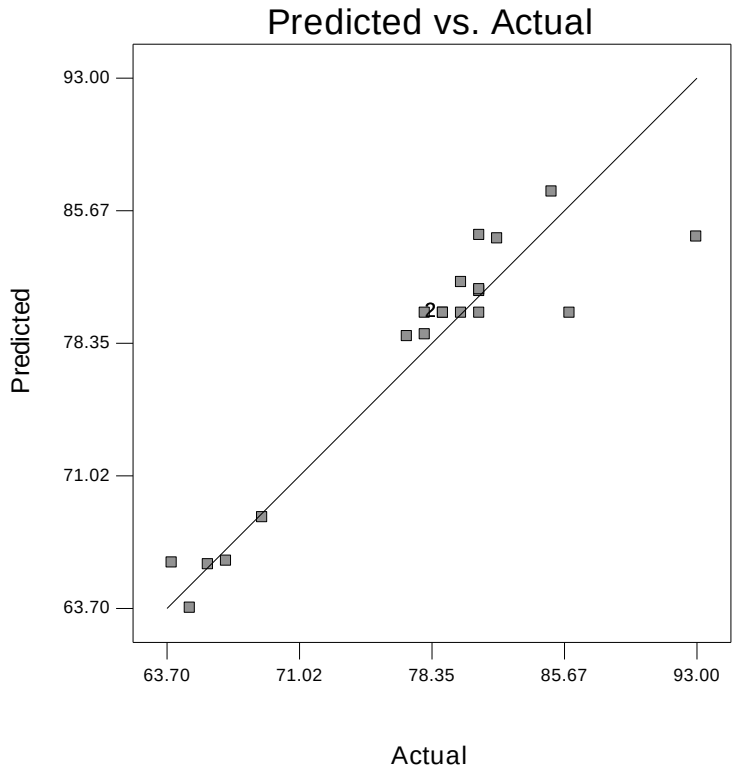

Figure 5.17: Actual data versus predicted data values for percentage of BT removed

In the next step, the predicted model was used to navigate the space defined by Central Composite Design (CCD). Figure 5.18 and 5.19 show the response surface plot which demonstrates the simultaneous effects of two factors on BT removal obtained from Eq. 5.1. For both figures, a significant decreasing trend in BT removal is shown with decreasing mass ratio (A) at a constant initial concentration (B) and temperature (C) values. Only slight increment was observed in BT removal when the initial concentration was decreased while on the other hand, slight decrement in BT removal was observed when temperature was decreased. Unfortunately, this result can be experiential by looking at the Eq. 5.1 alone which shows that mass ratio has a

greater effect on the response as compared to the initial concentration and temperature. Based on this analysis, it can be concluded that the initial concentration and temperature have little effect on BT removal from model oil. This might be attributed to the limitation effect of both initial concentration and temperature on sulfur-containing compounds extraction from model oil (*Mochizuki and Sugawara, 2008; Yu et al. 2011*).

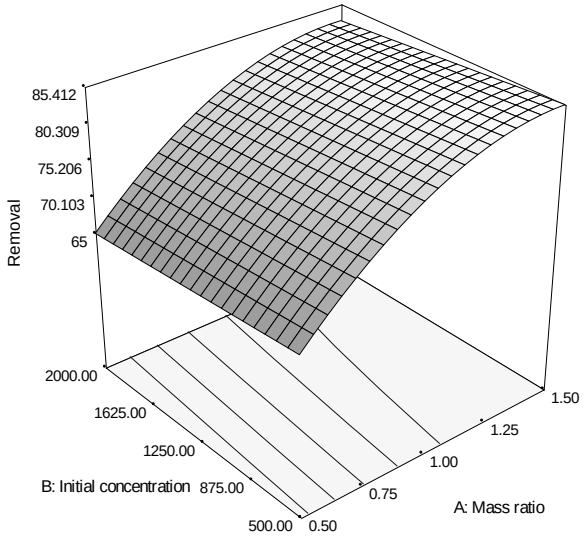

Figure 5.18: Response surface plot for BT removal with respect to mass ratio (A) and initial concentration (B)

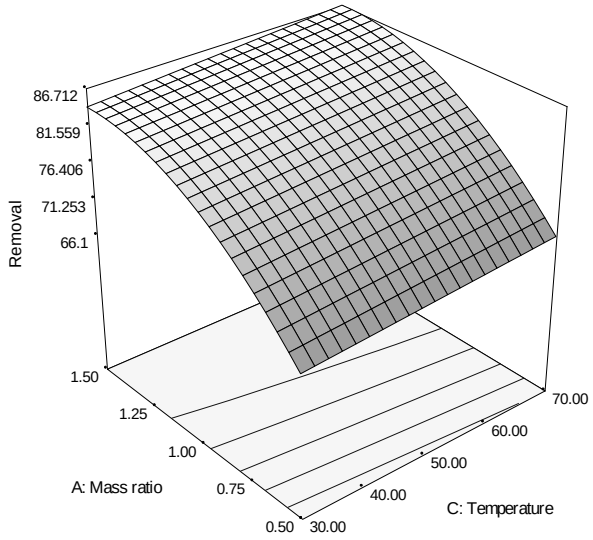

Figure 5.19: Response surface plot for BT removal with respect to mass ratio (A) and temperature (C)

5.5.2 Optimization Study

The optimum conditions for three independent variables namely mass ratio (A), initial concentration (B) and temperature (C) in removing BT were obtained using numerical optimization feature of Design Expert software. The optimization module in Design of Experiments (DoE) searches for the optimum values by combining all the factors that simultaneously satisfy the requirements placed on the factors and

response. All the factors and response with the respective upper and lower limits of experimental regions ideally have to satisfy the criteria defined for the desired optimum operation conditions, which are stated below in Table 5.6.

Table 5.6: The pre-set goal with the constraints for all the independent factors and response in numerical optimization

Variables	Ultimate goal	Experimental region	
		Lower limit	Upper limit
Factors			
Mass ratio (model oil/ILs)	Minimized	0.5	1.5
Initial concentration (ppm)	Maximized	500	2000
Temperature (°C)	Minimized	30	70
Response			
% Removal	Maximized	64	93

The ultimate goal of the operation conditions is to provide a high percentage in BT removal, minimizing the mass ratio and temperature while maximizing the initial concentration. The results obtained from the generated model show that, the optimum operation conditions for BT removal can be achieved by applying mass ratio (A) of 0.92 with initial concentration (B) of 2000 ppm at temperature (C) of 30°C. In order to validate this, the extraction experiments were carried out in triplicate using the proposed operation conditions, as shown in Table 5.7. The experimental result showed good agreement with prediction result as the percentage of BT removal is 76.50 as compared to predicted value of 76.03. Small error value and standard deviation justified that the observed value at these optimum operation conditions is in close agreement with predicted value, while the desirability plot shown in Figure 5.10 illustrates the trend of crucial factors, namely mass ratio (A) and initial concentration (B).

Table 5.7: Optimum operation conditions found by CCD for BT removal

A (model oil/ILs)	B (ppm)	C (°C)	% R Observed	% R Predicted	Error	S.D.
0.92	2000	30	76.65	76.03	0.62	±0.4384
			75.90		-0.13	±0.0919
			76.95		0.92	±0.6505

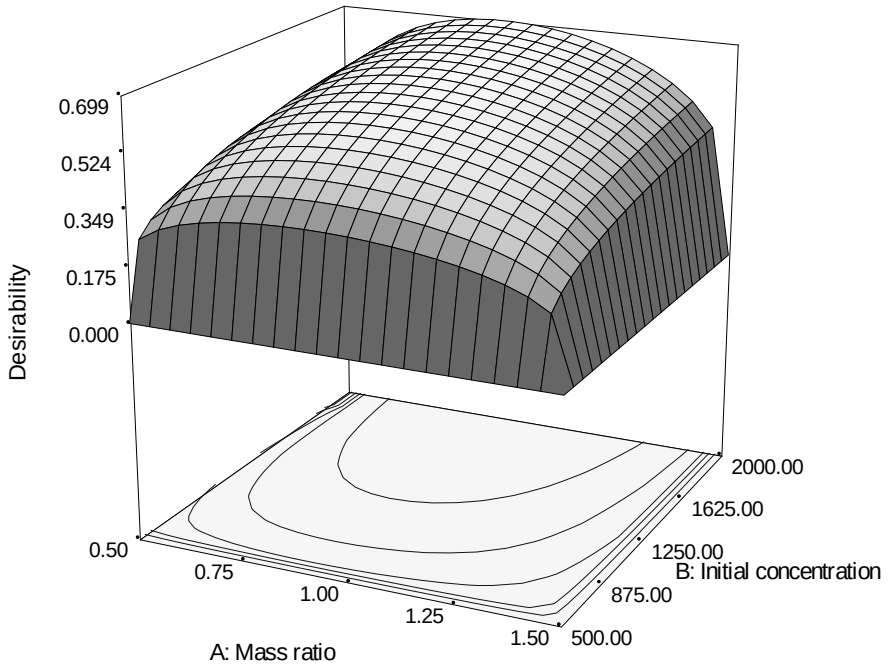

Figure 5.20: Desirability plot at temperature (C) of 30°C for obtaining desired optimum operation of mass ratio (A) and initial concentration (B)

5.5 Ternary Diagram Study

This part of the study of extractive desulfurization of diesel focuses on the removal of sterically hindered sulfur compound i.e. BT. Liquid-liquid equilibrium (LLE) data for the systems 1-butyl-3-methylimidazolium tricyanomethane ([bmim][TCM] + BT) + *n*-dodecane (*n*-C_{12}) or *n*-hexane (*n*-C_6) or *p*-xylene as the model oil were determined. Since temperature has little effect on the BT removal, the ternary diagram study was conducted at room temperature i.e. 25.5°C, due to the wide range temperature of studied ILs (~ 200°C) in liquid state.

The experimental LLE data for the ternary systems of ([bmim][TCM] + BT + *n*-C_{12}); ([bmim][TCM] + BT + *n*-C_6) and ([bmim][TCM] + BT + *p*-xylene) at 25.5°C and atmospheric pressure are reported in Table 5.8. The triangular diagram with tie-line for each system is plotted in Figure 5.21, 5.22 and 5.23, respectively. This set of plots provides a clear visualization of the changes of the immiscibility region shape as

a result of changing the model oil system i.e. *n*-C_{12}, *n*-C_6 and *p*-xylene. It is notable, however, that the mutual solubility of both hydrocarbons and ILs increases from *n*-C_{12} to *n*-C_6 to *p*-xylene system, with the pair (*n*-C_6 + [bmim][TCM]) and (*p*-xylene + [bmim][TCM]) eventually found to be partially miscible.

Table 5.8: Composition of the experimental tie-line ends and values of the solute distribution ratio (β) and selectivity (S) for the ternary systems ([bmim][TCM] + BT + *n*-C_{12}); ([bmim][TCM] + BT + *n*-C_6) and ([bmim][TCM] + BT + *p*-xylene) at 25.5°C

Oil phase			ILs phase				
X_1	X_2	X_3	X_1	X_2	X_3	β	S
([bmim][TCM] + BT + *n*-C_{12})							
0	0.02692	0.97308	0.57843	0.42157	0	15.66	-
0	0.02567	0.97433	0.68245	0.31755	0	12.37	-
0	0.02505	0.97495	0.75845	0.24155	0	9.64	-
0	0.02415	0.97585	0.79850	0.20150	0	8.34	-
0	0.02276	0.97724	0.88907	0.11093	0	4.87	-
([bmim][TCM] + BT + *n*-C_6)							
0.01552	0.03308	0.95140	0.44342	0.27654	0.28004	8.36	28.40
0.01156	0.03121	0.95723	0.55557	0.21908	0.22535	7.02	29.82
0.00983	0.03064	0.95953	0.61380	0.17152	0.21468	5.60	25.03
0.00904	0.02279	0.96817	0.68100	0.11419	0.20481	5.01	23.68
0.00582	0.01721	0.97697	0.79002	0.05985	0.15013	3.48	22.65
([bmim][TCM] + BT + *p*-xylene)							
0.06811	0.01680	0.91509	0.31774	0.23176	0.45050	13.80	28.03
0.04807	0.02284	0.92909	0.45141	0.17834	0.37024	7.81	19.60
0.02955	0.03113	0.93932	0.54466	0.12955	0.32579	4.16	11.99
0.02167	0.03397	0.94436	0.67411	0.08071	0.24518	2.38	9.17
0.01746	0.04067	0.94186	0.75134	0.04669	0.20197	1.15	5.36

The mole fractions of [bmim][TCM], BT and model oil (i.e. *n*-C_{12}, *n*-C_6 and *p*-xylene) are represented by X_1, X_2 and X_3

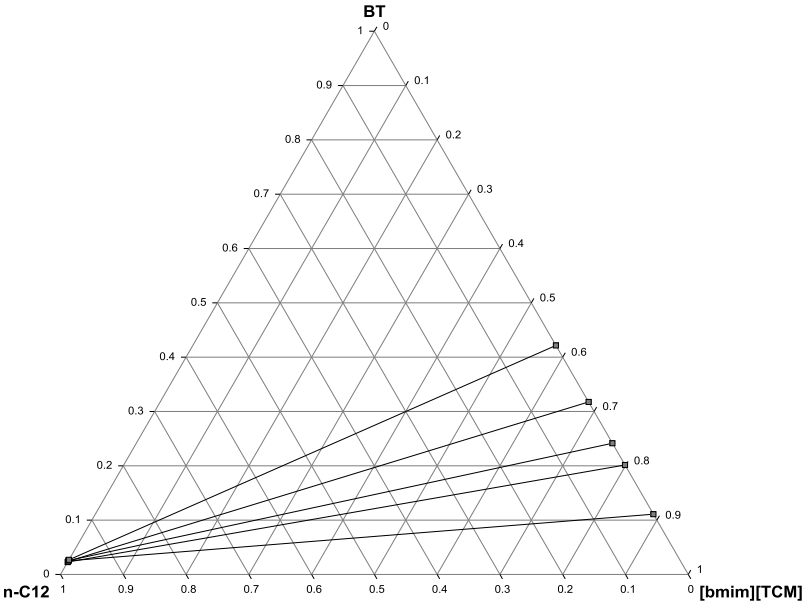

Figure 5.21: Experimental tie-lines for the LLE of the ternary system ([bmim][TCM] + BT + *n*-C_{12}) at 25.5°C

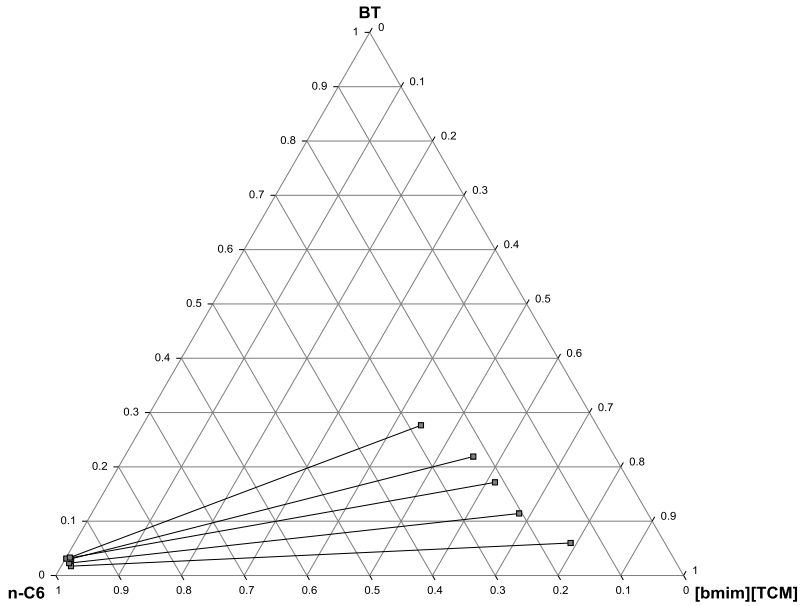

Figure 5.22: Experimental tie-lines for the LLE of the ternary system ([bmim][TCM] + BT + *n*-C_6) at 25.5°C

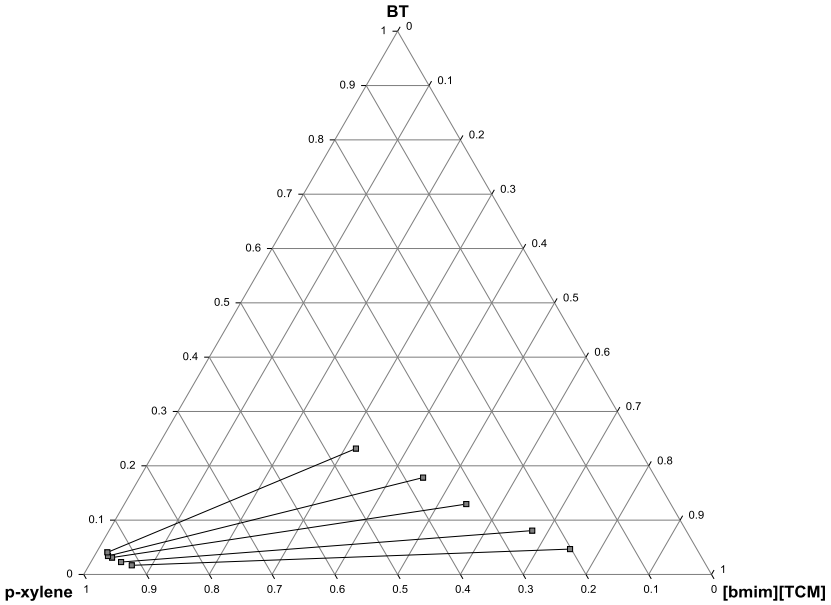

Figure 5.23: Experimental tie-lines for the LLE of the ternary system ([bmim][TCM] + BT + *p*-xylene) at 25.5°C

Together with the LLE data, Table 5.8 includes the corresponding values for the solute distribution ratio (β) and the selectivity (S), which are widely used parameters to characterize the suitability of ILs for liquid-liquid extraction (*Alonso*[a] *et al. 2007*). The β and S values can be calculated easily from the experimental compositions of the tie-line ends, according to the following expressions:

$$\boldsymbol{\beta} = \frac{\boldsymbol{X_1^{II}}}{\boldsymbol{X_2^{I}}} \tag{5.2}$$

$$\boldsymbol{S} = \frac{\boldsymbol{X_1^{II}}}{\boldsymbol{X_2^{I}}} \cdot \frac{\boldsymbol{X_1^{I}}}{\boldsymbol{X_1^{II}}} \tag{5.3}$$

where X is the molar fraction, the superscripts I and II refer to the oil-rich and ILs-rich phases, respectively, while the subscripts 1 and 2 refer to the hydrocarbon (i.e. *n*-C_{12}, *n*-C_6 and *p*-xylene) and the solute (i.e. BT), respectively.

An interesting fact observable from Figure 5.21, 5.22 and 5.23 is that, for all of the diagrams, the tie-lines show a positive slope throughout the immiscibility (two-phase)

region, which is a desirable feature for ILs to be an ideal extractant. Referring to Figure 5.21, the ternary system ([bmim][TCM] + BT + *n*-C_{12}) can be said to have a fairly good immiscible region as indicated by some area being partially covered by equilibrium tie-lines. In terms of miscibility of [bmim][TCM] and *n*-C_{12} phase, trace amount of [bmim][TCM] was found in the *n*-C_{12} phase and vice versa, which means that there is some carryover of the [bmim][TCM] into the oil phase as well as some oil is lost in the [bmim][TCM], which is one of the criteria for good extractant properties. However, the carryover amounts are minute that they are negligible. With respect to extraction of BT from *n*-C_{12} phase by [bmim][TCM], as the concentration of BT increases in *n*-C_{12} phase, the amount of BT extracted into the [bmim][TCM] phase is more than the amount that remained in the *n*-C_{12} phase. This is illustrated by the gradient of the tie-lines which favours BT extraction into [bmim][TCM] phase. This also indicates that [bmim][TCM] probably is a suitable extractant to be used for extraction of sulfur-containing compounds from diesel.

From the ternary systems in Figure 5.22 and 5.23, the miscibility region can be identified where significant amount of *n*-C_6 and *p*-xylene were found in the [bmim][TCM] phase. This means that unlike *n*-C_{12}, *n*-C_6 and *p*-xylene have a very high solubility with [bmim][TCM] which will affect the overall immiscibility region of the ternary systems with BT. In practical sense, this would actually dissolve some sort of short aliphatic chain (i.e. *n*-heptane and *n*-octane) and a lot of aromatics (i.e. benzene and toluene) into the ILs phase, and would result in loss of hydrocarbons during extractive desulfurization of diesel.

5.6 Extractive Desulfurization on Model Fuel

Removing sulfur-containing compounds without removing hydrocarbons, especially aromatic, is essential in extraction process as the aromatic hydrocarbons are important components for maintaining the quality of fuel (*Nie et al. 2008*). As such, an ideal extractive solvent that is capable to selectively extract only sulfur-containing compounds is desired. The results of extractive desulfurization study on five model fuel namely benzene/BT mixtures in *n*-C_{12}, *p*-xylene/BT mixtures in *n*-C_{12}, benzene/DBT mixtures in *n*-C_{12}, *p*-xylene/DBT mixtures in *n*-C_{12} and BT/DBT

mixtures in *n*-C_{12} are shown in Table 5.10. The extractive desulfurization was conducted at the optimized condition (stirring speed - 500rpm, extraction time - 30 minutes, mass ratio of model fuel to ILs - 1:1 and temperature was at room temperature), which have been previously identified. Five selected ILs were used in this study, namely [bmim][OSO_4], [bmim][DCA], [bmim][SCL], [bmim][BZT] and [bmim][TCM] based on the previous experimental results that showed these ILs to have the highest performance in removing BT from *n*-C_{12}. The typical HPLC and GC chromatograms for this study are depicted in the Appendix D for BT/*p*-xylene mixture in *n*-C_{12}, before and after extraction using [bmim][TCM].

In general, Table 5.9 shows that all tested ILs extracted BT and DBT including aromatic hydrocarbons without noticeable mutual hindrance. The K_D values for BT and DBT are remarkably high whereas benzene and *p*-xylene have low values ranging from 0.190 to 0.818. It is worthy to note that, the K_D values for sulfur-containing compounds i.e. BT and DBT remain constant in all systems regardless of different type of aromatic hydrocarbon present in the systems. Therefore for each system, these tabulated data need to be presented in bar graph for better evaluation and observation.

Figure 5.24 indicates that [bmim][OSO_4] selectively extracts sulfur-containing compounds (BT and DBT) from *n*-C_{12} independent of any interruption from aromatic hydrocarbons. The selectivity ratio of sulfur-containing compounds and aromatic hydrocarbons, $S_{Or/HC}$ which is defined as the ratio of the partition coefficient of sulfur-containing compounds against aromatic hydrocarbon was calculated from Eq. 5.4. The calculated ratios for BT/benzene, BT/*p*-xylene, DBT/benzene and DBT/*p*-xylene in *n*-C_{12} are 3.5, 8.6, 4.0 and 9.5, respectively.

$$\boldsymbol{S_{Or/HC} = K_d \text{ (sulfur-containing compound)} / K_d \text{ (aromatic hydrocarbon)}} \quad (5.4)$$

For instance, based on the selectivity ratio value, the selectivity towards BT or DBT decreases in benzene system compared to *p*-xylene system due to the degree of miscibility of benzene in [bmim][OSO_4] phase.

Table 5.9: Tabulation of % removal and K_d value of model fuels extracted by five selected ILs

Model fuel	% removal		K_d value	
	HC	S	HC	S
		[bmim][OSO_4]		
BT/benzene in *n*-C_{12}	33	63	0.493	1.703
BT/*p*-xylene in *n*-C_{12}	19	67	0.235	2.030
DBT/benzene in *n*-C_{12}	36	69	0.563	2.226
DBT/*p*-xylene in *n*-C_{12}	19	69	0.235	2.226
BT/DBT in *n*-C_{12}	-	65/68	-	1.857/2.125
		[bmim][DCA]		
BT/benzene in *n*-C_{12}	32	70	0.471	2.333
BT/*p*-xylene in *n*-C_{12}	18	71	0.220	2.448
DBT/benzene in *n*-C_{12}	29	75	0.408	3.000
DBT/*p*-xylene in *n*-C_{12}	17	77	0.205	3.348
BT/DBT in *n*-C_{12}	-	69/75	-	2.226/3.000
		[bmim][SCL]		
BT/benzene in *n*-C_{12}	39	70	0.639	2.333
BT/*p*-xylene in *n*-C_{12}	22	72	0.282	2.571
DBT/benzene in *n*-C_{12}	45	75	0.818	3.000
DBT/*p*-xylene in *n*-C_{12}	30	74	0.429	2.846
BT/DBT in *n*-C_{12}	-	71/74	-	2.448/2.846
		[bmim][BZT]		
BT/benzene in *n*-C_{12}	40	70	0.667	2.333
BT/*p*-xylene in *n*-C_{12}	23	73	0.299	2.704
DBT/benzene in *n*-C_{12}	41	71	0.695	2.448
DBT/*p*-xylene in *n*-C_{12}	24	70	0.316	2.333
BT/DBT in *n*-C_{12}	-	70/74	-	2.333/2.846
		[bmim][TCM]		
BT/benzene in *n*-C_{12}	35	78	0.538	3.545
BT/*p*-xylene in *n*-C_{12}	17	77	0.204	3.348
DBT/benzene in *n*-C_{12}	37	80	0.587	4.000
DBT/*p*-xylene in *n*-C_{12}	16	80	0.190	4.000
BT/DBT in *n*-C_{12}	-	78/79	-	3.545/3.762

HC – hydrocarbon compound i.e. benzene and *p*-xylene
S – sulfur-containing compound i.e. BT and DBT

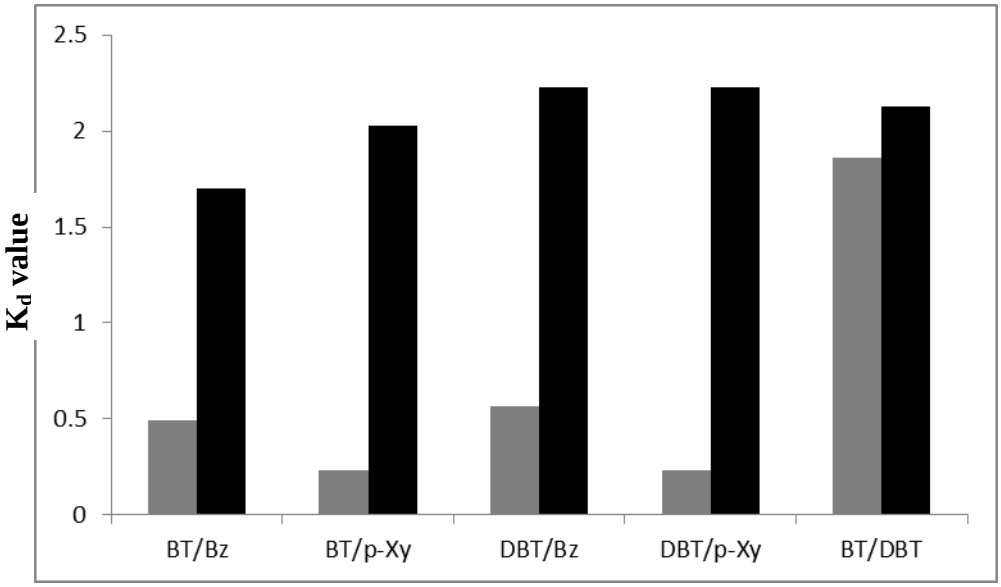

Figure 5.24: Extractive desulfurization performance of [bmim][OSO_4] on model fuel

In comparison to [bmim][OSO_4], [bmim][DCA] selectively extracts more sulfur-containing compounds and less aromatic hydrocarbons from *n*-C_{12} as indicated in Figure 5.25. The highest extraction of sulfur-containing compounds from the *p*-xylene system was 77% removal. In *p*-xylene systems, both sulfur compounds depict high selectivity ratio as compared to benzene system which followed the same trend as previously shown by [bmim][OSO_4] as the extractant. The selectivity ratio values when [bmim][DCA] was the extractant are 5.0, 11.1, 7.4 and 16.3 for BT/benzene, BT/*p*-xylene, DBT/benzene and DBT/*p*-xylene in *n*-C_{12}, respectively.

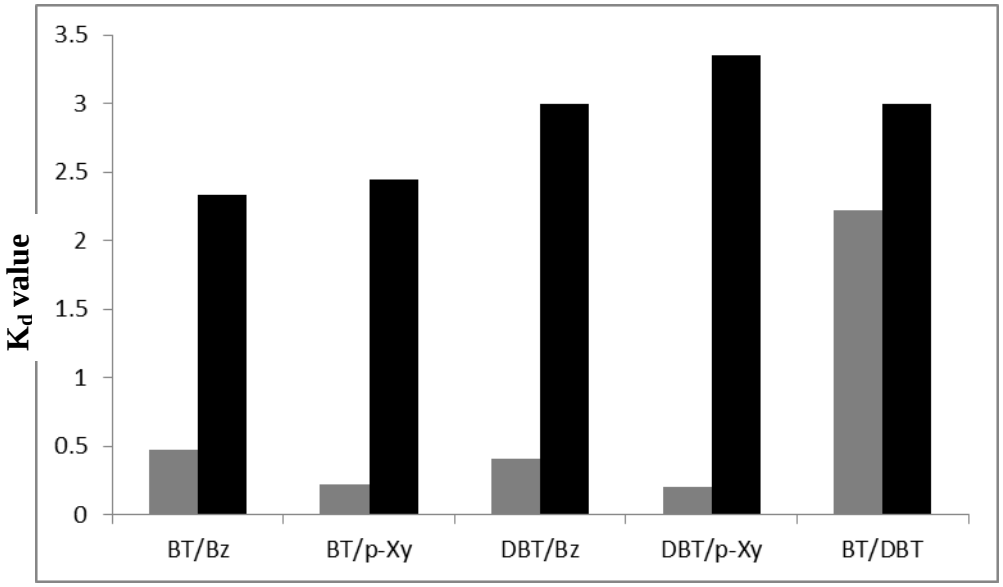

Figure 5.25: Extractive desulfurization performance of [bmim][DCA] on model fuel

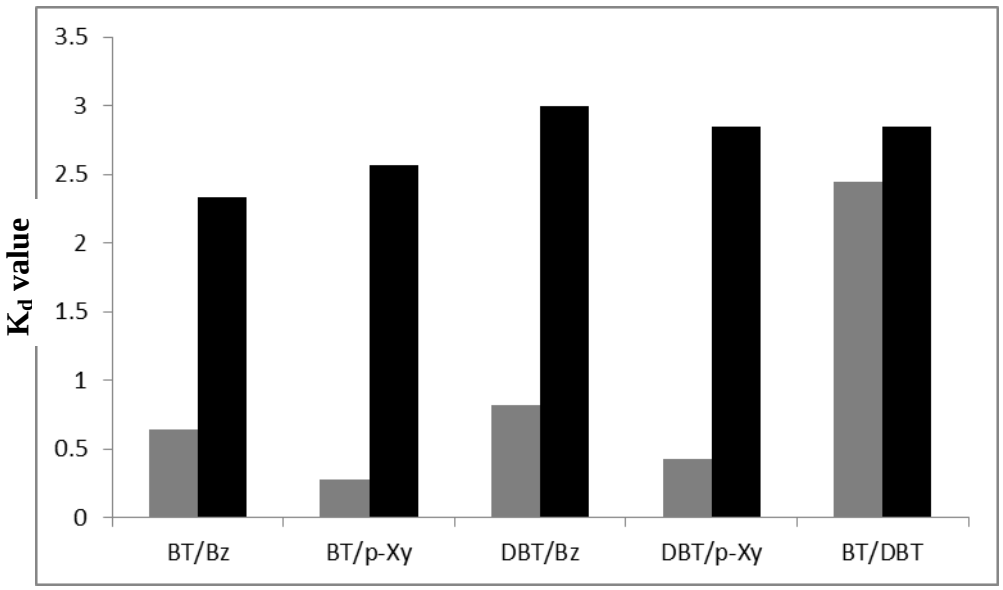

Figure 5.26: Extractive desulfurization performance of [bmim][SCL] on model fuel

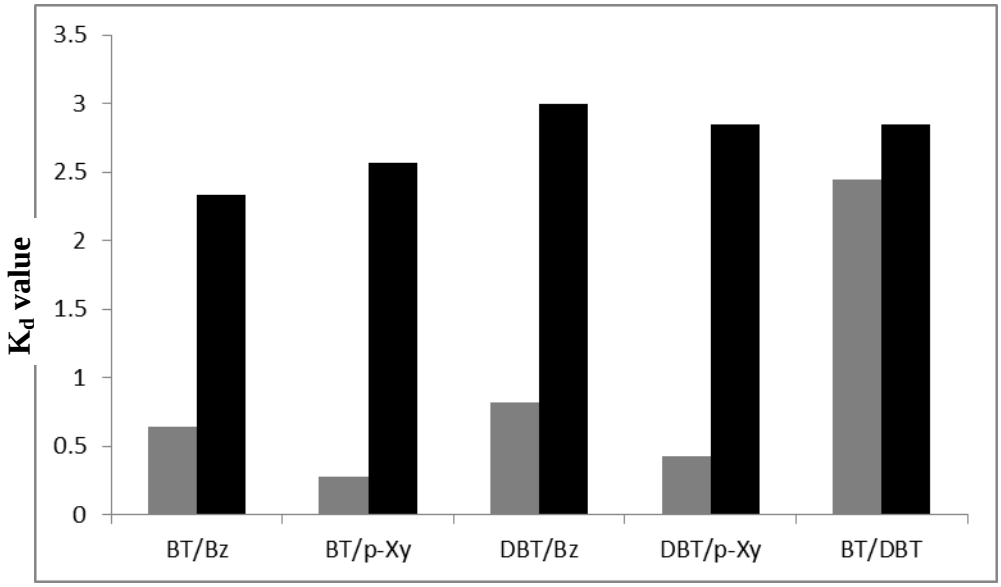

Figure 5.27: Extractive desulfurization performance of [bmim][BZT] on model fuel

The performance of extractive desulfurization of model fuel using [bmim][SCL] and [bmim][BZT] are shown in Figures 5.26 and 5.27, respectively. Both [bmim][SCL] and [bmim][BZT] have the same selectivity ratio for BT/benzene, BT/*p*-xylene, DBT/benzene and DBT/*p*-xylene in *n*-C_{12}, which are 3.7, 9.1, 3.7 and 6.6, respectively, even though [bmim][BZT] show slightly higher extraction yield of sulfur-containing compounds compared to [bmim][SCL].

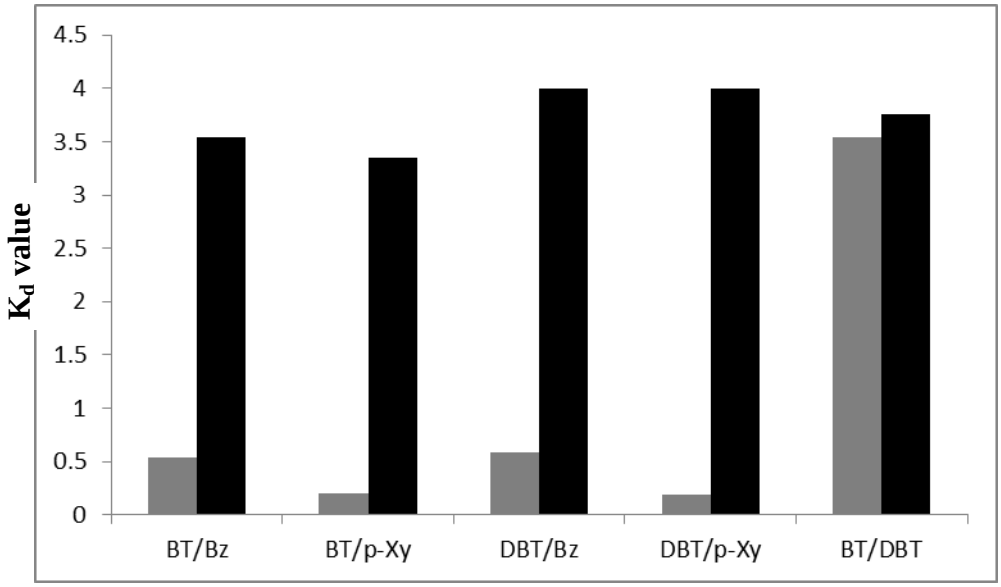

Figure 5.28: Extractive desulfurization performance of [bmim][TCM] on model fuel

In Figure 5.28, the performance of extractive desulfurization using [bmim][TCM] as the extractant was evaluated. It seems that [bmim][TCM] presents a similar trend as observed earlier for [bmim][OSO_4], [bmim][DCA], [bmim][SCL] and [bmim][BZT] where the extraction favors sulfur-containing compounds rather than the aromatic hydrocarbons. The selectivity ratios are 6.6, 16.4, 6.8 and 21.1 for BT/benzene, BT/*p*-xylene, DBT/benzene and DBT/*p*-xylene mixture in *n*-C_{12}, respectively. Among the tested ILs, [bmim][TCM] shows the highest selectivity ratio value in both benzene and *p*-xylene systems. High selectivity ratio is one of the desirable features for ILs to be an ideal extractant. At this point, [bmim][TCM] is still the suitable candidate for extractive desulfurization.

It is interesting to note that, [bmim][TCM] has specific capacity for sulfur-containing compounds and aromatic hydrocarbons with the K_d values being constant and independent of its concentration. The study on percentage removal and K_d of sulfur-containing compound i.e. BT and DBT with different concentration of *p*-xylene extracted by [bmim][TCM] from *n*-C_{12} are tabulated in Table 5.10. As can be seen in Table 5.10, the increase in *p*-xylene concentration did not influence the removal percentage of both BT and DBT, and the K_d values are not affected. This results indicate that [bmim][TCM] is particularly selective for sulfur-containing compounds rather than aromatic hydrocarbons in *n*-C_{12}. Figure 5.29 shows the trends which depict more clearly the K_d value of BT and DBT as a function of initial mole fraction of *p*-xylene in *n*-C_{12}.

Table 5.10: Removal percentage and partition coefficient (K_d) of BT and DBT with different concentration of *p*-xylene extracted by [bmim][TCM] from *n*-C_{12}

Volume ratio	**% removal**		**K_d value**	
(*n*-C_{12}/ aromatic hydrocarbon)	HC	S	HC	S
BT/*p*-xylene in *n*-C_{12}				
8/2	17	77	0.204	3.348
7/3	18	77	0.220	3.348
6/4	18	76	0.220	3.167
5/5	20	77	0.250	3.348
DBT/*p*-xylene in *n*-C_{12}				
8/2	16	80	0.190	4.000
7/3	19	79	0.235	3.762
6/4	18	79	0.220	3.762
5/5	20	79	0.250	3.762

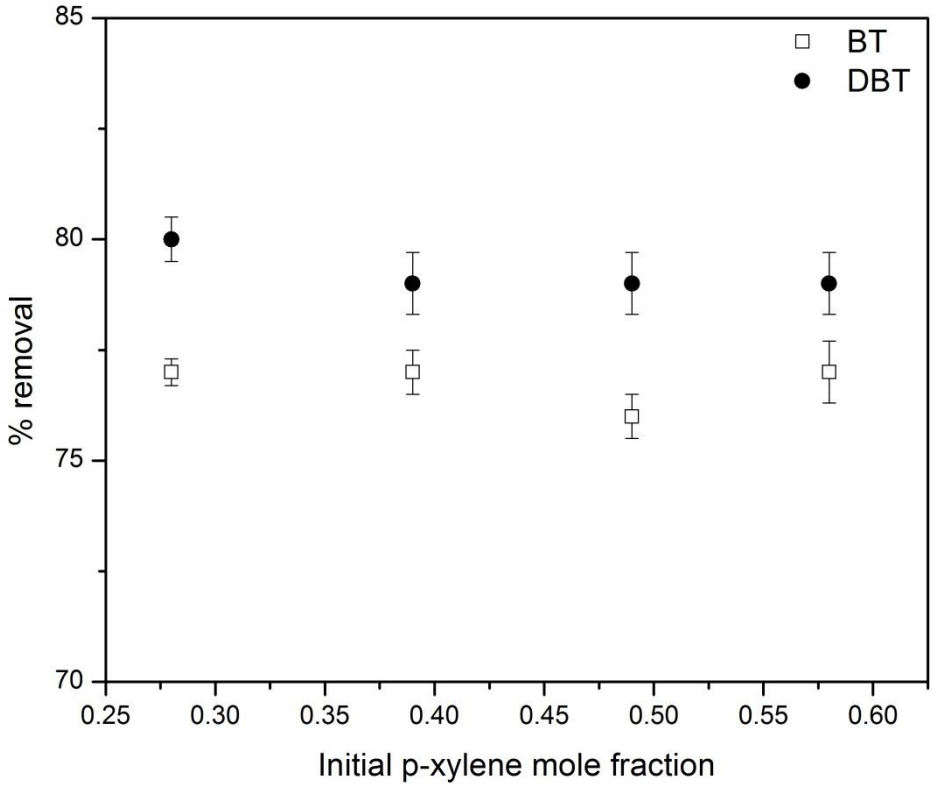

Figure 5.29: K_d values for BT and DBT with [bmim][TCM] as extractant on model fuel system

It appears that the removal performance is favored for molecules with a higher π-electron density where in this case, DBT and BT possessed the highest π-electron density followed by benzene, and *p*-xylene (*Gao et al. 2008; Zhang and Zhang, 2002; Eßer et al. 2004; Su et al. 2004; Sidhpuria and Parikh, 2004*). Zhang and Zhang

(2002) in their investigation observed that, aromatic compounds which rendered the highest π-electron density demonstrated stronger interaction with BF_4-based and PF_6-based ILs. This drawback may suggest that diesel will lose some of the aromatic hydrocarbons during the extractive desulfurization process using ILs.

However, the capability of ILs to selectively remove benzene compounds besides organosulfur from petroleum products, especially in diesel may render some added advantage. Benzene is highly carcinogenic, and due to worsening air pollution and concerns on exposure to the public during a self-service automobile refueling, some countries have imposed more stringent product specifications, which particularly require lower content of benzene and organosulfur compounds in fuels (*Yasuo and Yoshiki, 1997*). From this point of view, ILs can be designed for removing organosulfur and at the same time extract some carcinogenic aromatic hydrocarbons from petroleum products.

5.7 Extractive Desulfurization Study on Commercial Diesel

Two types of commercial diesel were also treated with these ILs namely Diesel A and Diesel B, and their original total sulfur content was 1128 ppm and 1357 ppm, respectively. Diesel A and Diesel B were subjected to GC-MS for compound speciation and initial concentration evaluation, where seven compounds were identified for extraction process. Three ILs were selected which were [bmim][OSO_4], [bmim][DCA] and [bmim][TCM]. Both [bmim][SCL] and [bmim][BZT] were not evaluated due to their high in miscibility on diesel.

5.7.1 Speciation and Extraction Performance Study

Diesel A and Diesel B were extracted at room temperature using [bmim][OSO_4], [bmim][DCA] and [bmim][TCM] as extractant. The GC-MS chromatograms before extraction of both Diesel A and Diesel B are shown in the Appendix D (D15 and D 16). The concentration of each identified species is shown in Table 5.11 for Diesel A before and after the extraction process using the three selected ILs.

Table 5.11: Concentration of identified species in Diesel A after extraction with three selected ILs

	***n*-C_6**	***n*-C_{12}**	**benzene**	**toluene**	***p*-xylene**	**BT**	**DBT**
Initial conc. (ppm) in Diesel A	65	3250	56	274	895	68	233
After extraction using [bmim][OSO_4]	56	3221	19	164	589	0	11
After extraction using [bmim][DCA]	54	3234	14	159	567	0	0
After extraction using [bmim][TCM]	53	3211	0	157	551	0	0

All three ILs showed a remarkable capacity for removing sulfur-containing compounds (BT and DBT) from Diesel A. 100% removal was achieved by both [bmim][TCM] and [bmim][DCA], while 95% removal of DBT was achieved using [bmim][OSO_4]. Besides sulfur-containing compounds, aromatic hydrocarbons were also detected being removed during the extraction process. For example, there is 100% removal of benzene in Diesel A using [bmim][TCM] while [bmim][DCA] and [bmim][OSO_4] gave 75 and 66% of benzene removal. Other species including toluene and *p*-xylene were also removed during the extraction process but in lower removal percentage compared to benzene. Aliphatic hydrocarbons such as *n*-hexane (*n*-C_6) and *n*-C_{12} were also slightly removed during the extraction as shown in Figure 5.30.

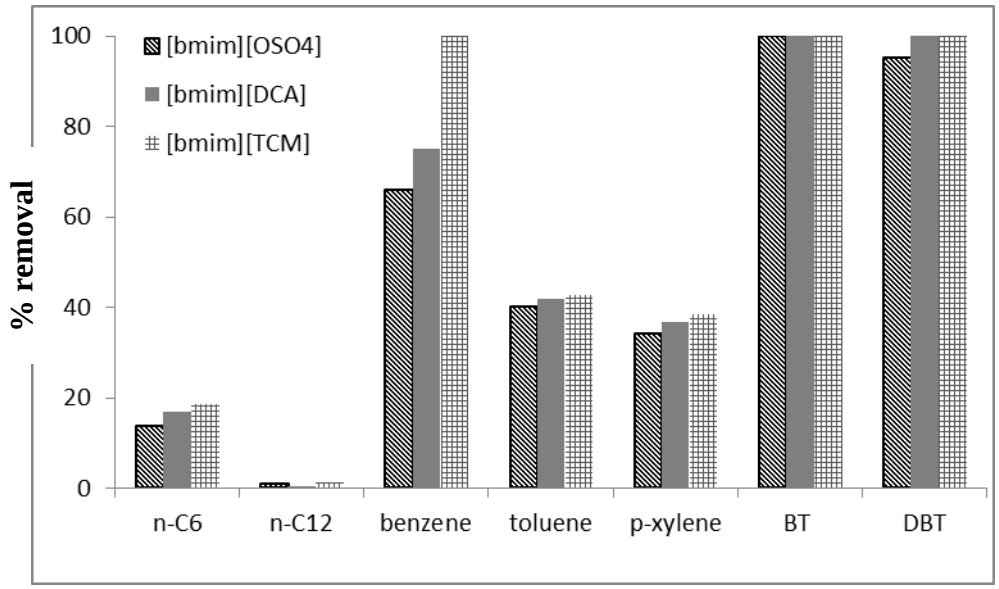

Figure 5.30: Percentage removal of identified species in Diesel A, a comparison of three selected ILs at room temperature

For Diesel B, the concentration of each identified species is shown in Table 5.12. Similarly, the concentration of sulfur-containing compounds (BT and DBT) drastically dropped down to zero concentration mostly after extraction by [bmim][TCM]. For [bmim][DCA] case, DBT was observed to be completely removed, but 16 ppm of BT still leftover in Diesel B after 30 minutes of extraction. This may be explained as due to [bmim][DCA] that had reached saturation point, thus unable to extract the remaining BT. On the other hand, [bmim][OSO_4] depicted a high performance in removing sulfur-containing compounds in Diesel B, achieving 86 and 94% for BT and DBT, respectively.

Table 5.12: Concentration of identified species in Diesel B after extraction with three selected ILs

	***n*-C_6**	***n*-C_{12}**	**benzene**	**toluene**	***p*-xylene**	**BT**	**DBT**
Initial conc. (ppm) in Diesel B	104	3240	47	174	365	116	587
After extraction using [bmim][OSO_4]	83	3214	13	88	281	16	33
After extraction using [bmim][DCA]	84	3240	11	86	274	16	0
After extraction using [bmim][TCM]	72	3158	0	77	262	0	0

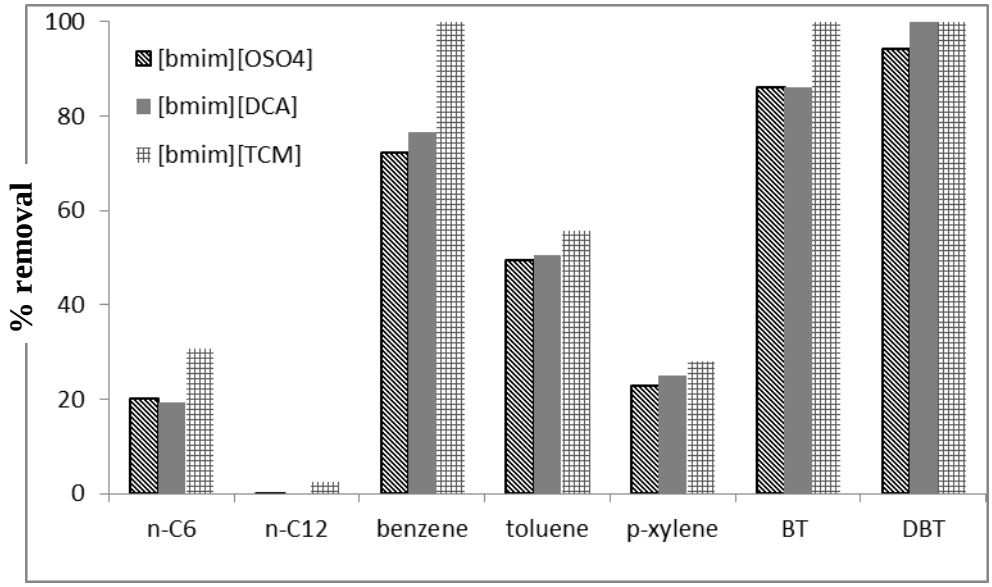

Figure 5.31: Percentage removal of identified species in Diesel B, a comparison of three selected ILs at room temperature

In Figure 5.31, benzene is observed to be completely eliminated from Diesel B with [bmim][TCM] as the extractant, while by using [bmim][DCA] and [bmim][OSO_4], the removal of benzene achieved was 77 and 72%, respectively. The removal of other aromatic hydrocarbons slowly decreases from toluene to *p*-xylene as the number of alkyl side chain increases. The alkyl side chain reduces the π-π interaction between the extractant (ILs) and aromatic hydrocarbons. Meanwhile in aliphatic hydrocarbons, the removal was largely due to *n*-C_6 where this short chain aliphatic was found experimentally to be partially miscible with ILs. For *n*-C_{12}, the removal was almost negligible ranging between 0.5 to 2% removals.

Since the sulfur-containing compounds still remained in both Diesel A and Diesel B after the one step extraction process, whether they are the species already identified by GC-MS or others that were measured using Total Sulfur Analyzer, the number of extraction cycle needs to be determined in order to reduce the sulfur content to ultra-low level in order to meet the new specification for commercial diesel. For calculation purposes, bear in mind that one ppm of total sulfur concentration is equivalent to 4.19 ppm of BT or 5.76 ppm of DBT.

5.7.2 Extraction Cycle Study

The extractive desulfurization cycle of Diesel A and Diesel B with [bmim][TCM] at room temperature was assessed. The contents of total sulfur after various cycles of extractions are illustrated in Figure 5.32.

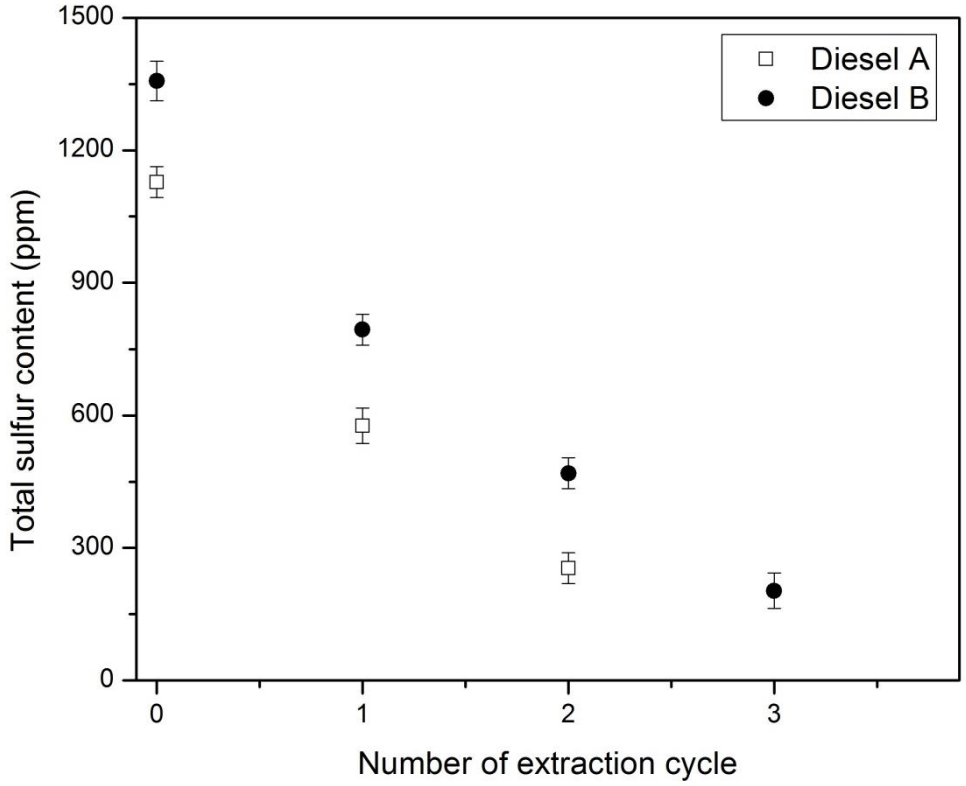

Figure 5.32: Total sulfur concentration in Diesel A and Diesel B after multiple extraction with [bmim][TCM] at room temperature
(Conditions: Stirring speed – 500 rpm, extraction time – 30 min, mass ratio ILs/model oil – 1/1, room temperature, initial total sulfur concentration in Diesel A – 1128 ppm, initial total sulfur concentration in Diesel B – 1357 ppm)

In Figure 5.32, the total sulfur concentration of Diesel A decreased from 1128 ppm to 254 ppm after two extraction cycles while in Diesel B, three extraction cycles are required to reduce from 1357 ppm to 203 ppm. Thus, the total sulfur concentration in Diesel A that was removed by first and second cycles are 48.85 and 77.48%, respectively. For Diesel B, the total sulfur concentration that was removed by first, second and third cycles are 41.49, 65.44 and 85.04%, respectively.

In Malaysia now, the target is to bring down the total sulfur concentration in diesel to 50 ppm, but the lowest detectable concentration in this work is 200 ppm due to the limitation of the equipment. By referring to the results of the multiple extraction, [bmim][TCM] is possible to achieve below than 50 ppm of total sulfur concentration using five extraction cycles based on its performance as an extractant for extractive desulfurization.

On the other hand technically, in order to confirm there is no cross-miscibility between [bmim][TCM] and diesel after extraction, [bmim][TCM] phase was subjected to density meter for this matter clarification. Figure 5.33 shows the results of this analysis. There is negligible differences value ~ 0.21% in [bmim][TCM] phase density have been detected before and after extraction cycle. It can be deduced from this result, there is very small or insignificant amount of diesel miscible in [bmim][TCM] phase.

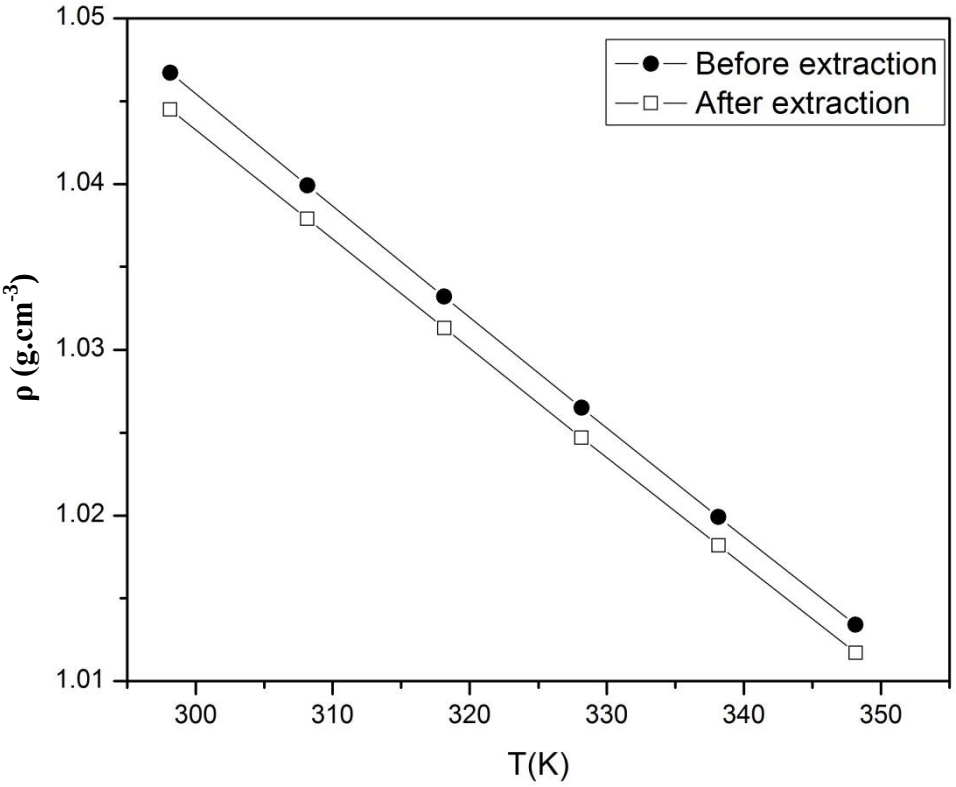

Figure 5.33: Density differences of [bmim][TCM] value against the function of temperature

5.8 Regeneration Study

ILs are known as environmentally benign solvents due to their attractive properties which do not pose any threats to the environment, and one of which is its recyclable nature. Besides addressing cost and disposal concerns, the regeneration of ILs needs to be studied in order to assess its feasibility for up-scale applications [Nie et al. 2008]. In general, ILs has higher density than organic liquids, therefore, many ILs may form a separate phase when in contact with organic liquids. This feature makes the ILs possible to be regenerated (*Nefedieva et al. 2011; Nie et al. 2007*).

5.8.1 Re-extraction Technique using water/*n*-heptane

One of the promising techniques is precipitation of sulfur-containing compounds from spent ILs phase by water, and then the ILs in extracted from from water/ILs mixture using *n*-heptane. Finally, the ILs/*n*-heptane mixture is distilled to recover the ILs. For this regeneration study, the spent [bmim][TCM] was stirred with water and *n*-heptane for several minutes. The lower phase, mostly consisted of water/ILs mixture was separated from *n*-heptane and was subjected to rotary evaporator. After three hours of rotary evaporation, the water and ILs was separated. Then the total sulfur content of the *n*-heptane phase (after first separation process) and ILs phase (after rotary evaporator) were measured using Total Sulfur Analyzer (TSA); the results are tabulated in Table 5.13.

Table 5.13: Total sulfur in *n*-heptane and ILs phase before and after regeneration

	Total Sulfur Concentration
Spent [bmim][TCM] before recycling process	2235 ppm
Fresh *n*-heptane	-
Upper phase (*n*-heptane)	546 ppm
Lower phase ([bmim][TCM])	449 ppm

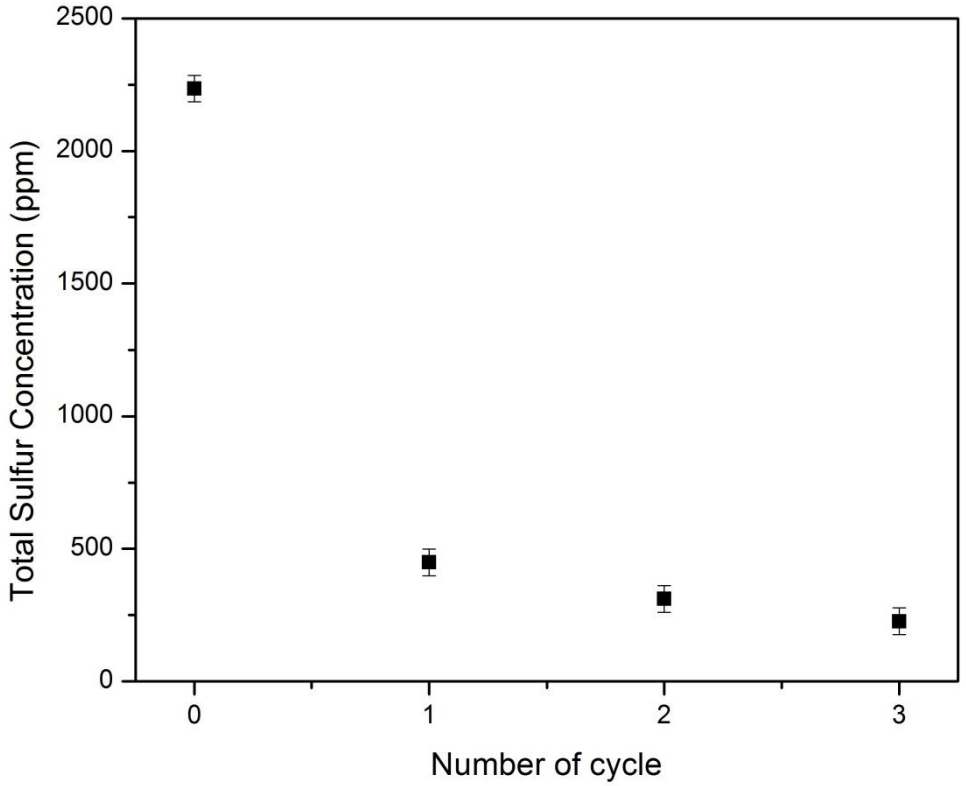

Figure 5.34: Effect of recycling on total sulfur concentration in [bmim][TCM]

Based on Table 5.13, the total sulfur concentration in [bmim][TCM] before regeneration was 2235 ppm; after first cycle of recycling process, this concentration was reduced to 449 ppm, a reduction of about 79.91%. While 546 ppm was detected in *n*-heptane phase, which indicates that 1240 ppm (~55%) was removed through filtration process. This recycling process was evaluated further by repeating the above process up to three cycles, and their results are shown in Figure 5.34. The leftover of the total sulfur concentration in [bmim][TCM] after second and third cycle of recycling process was 311 and 227 ppm, respectively. Based on the results, a further reduction of sulfur is highly possible at higher number of regeneration cycle.

Meanwhile, the percentage of sulfur removed from [bmim][TCM] phase had drastically dropped from 79.91% for the first cycle to 30.73% and 27.01% for second and third cycle, respectively. This shows that it is more difficult to remove remaining sulfur left [bmim][TCM] by regeneration method as the concentration of sulfur becomes lower. Thus, another promising technique for removing low concentration

sulfur from spent ILs i.e. electrochemical technique was investigated as part of the regeneration study.

5.8.2 Electrochemical Technique

In order to evaluate the electrochemical technique for recycling process, the selected five ILs namely [bmim][OSO_4], [bmim][DCA], [bmim][SCL], [bmim][BZT] and [bmim][TCM] were analysed for electrochemical stabilities using cyclic voltammetry. Due to inconsistent results of both [bmim][SCL] and [bmim][BZT], these ILs were omitted from further study. The electrochemical stability study was carried out on the other three and their electrochemical stabilities are shown in Figure 5.35.

Figure 5.35 shows the cyclic voltammograms for three types of ILs containing sulfate, nitrate and thiocyanate group. The "window" of the electrochemical stability of [bmim][DCA], [bmim][OSO_4] and [bmim][TCM] are found to be 3.5V (-1.0 to 2.5V), 3V (-1.5 to 1.5V) and 2.2V (-1.5 to 0.7V), respectively. From the literature, it was observed that the area of oxidation or electropolymerization of BT occurred as the anodic current increases in the anodic region, as indicated by $\mathbf{E_{pc}}$. As proposed by Schucker and Baird (2001), the suitable potential should be conducted between 1.0 to 2.5V for thiophene derivatives. Meanwhile, Nefedieva et *al*. (2011), found that the appropriate potential of [bmim][BF_4] for removing BT was 2.0V, where oxidation occurred in the anodic region. Therefore, further cycle should be proceeded with [bmim][DCA] only.

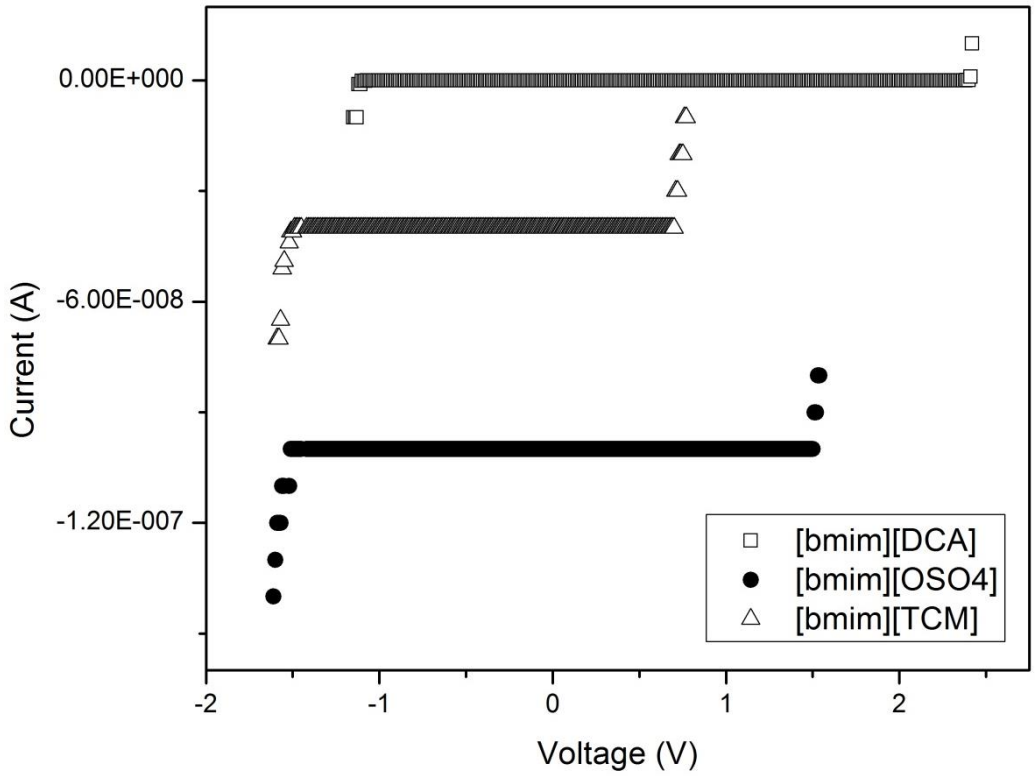

Figure 5.35: Cyclic voltammogram of [bmim][DCA], [bmim][OSO_4] and [bmim][TCM] relative to Ag/AgCl quasi-reference electrode, with glassy carbon as working electrode and Pt as counter electrode at 25 °C

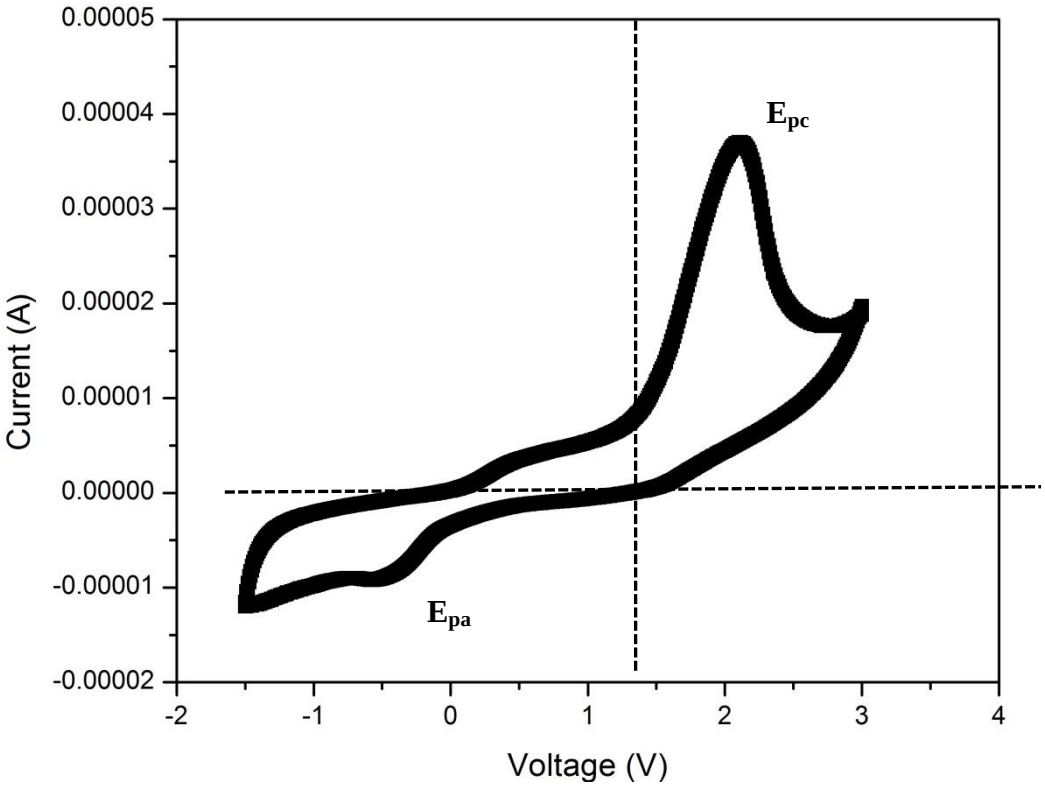

Figure 5.36: Cyclic voltammogram of BT in [bmim][DCA] with scan rate 1 mV s^{-1}

The anodic current was observed to increase (see the peak at $\mathbf{E_{pc}}$ = 2.0V in Figure 5.36) from the stationary value after preliminary stirring. There was a small peak area of reduction in the cathodic region at $\mathbf{E_{pa}}$ = -0.5V which possibly may be due to water content in the [bmim][DCA] + BT. The concentration of BT in spent [bmim][DCA] slowly dropped per minute, as illustrated in Figure 5.37. Within 24 hours, the total sulfur concentration in [bmim][DCA] had completely deposited at the glassy carbon electrode. The structure of the deposit at the glassy carbon electrode was confirmed as BT structure using FTIR spectroscopy, the spectrum is shown in Figure 5.38. This result illustrates that electrochemical technique is a promising technique for recycling spent ILs.

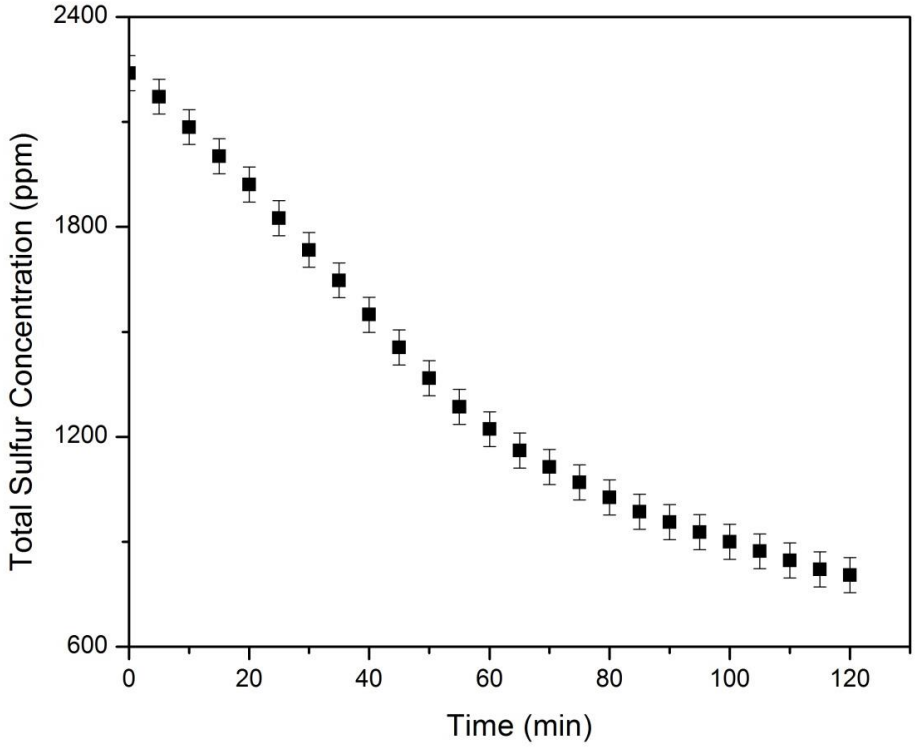

Figure 5.37: Total sulfur concentration in spent [bmim][DCA] over time during the electrochemical technique

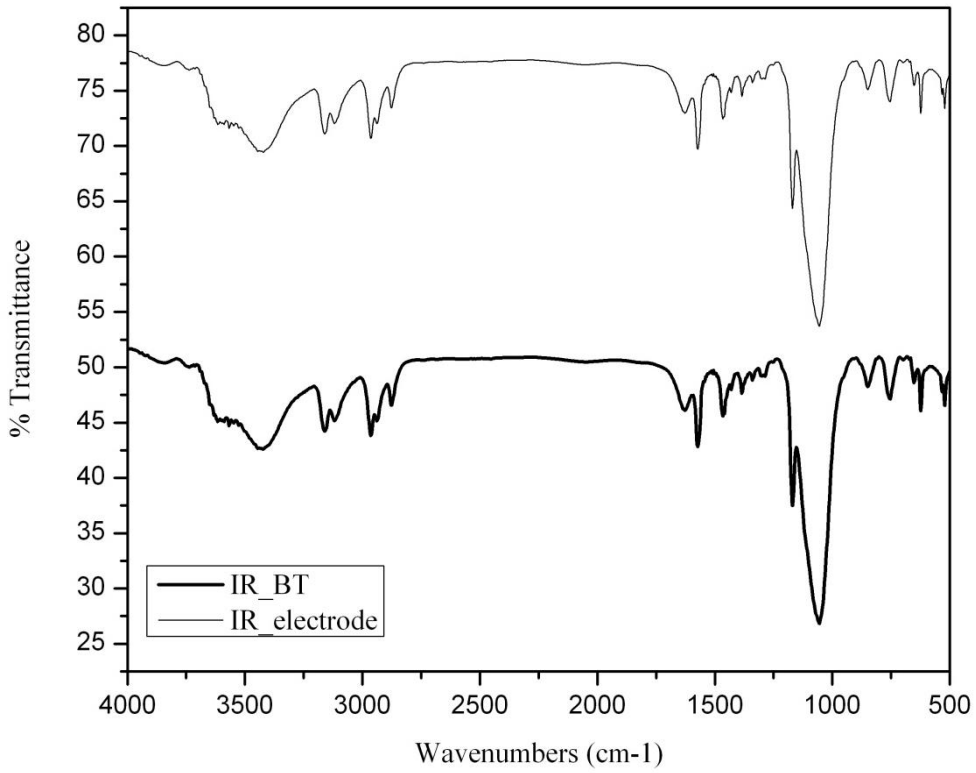

Figure 5.38: FTIR spectra of pure BT (IR_BT) and deposited BT (IR_electrode) at glassy carbon electrode